Silos Structural Response to Blast Loading

Yehya Temsah[1], Ali Jahami[1]*, Charles Aouad[2]

[1] Faculty of Engineering, Beirut Arab University, Beirut, Lebanon

[2] Astrophysics Research Institute, Liverpool John Moores University, Liverpool, UK

* Corresponding Author email: a.jahmi@bau.edu.lb

Abstract

Extensive research work has been conducted to study the structural behavior of silos for various static load types; namely the grain load compression phases inside the silos and the thermal loads. However, very few investigations were related to the effect of different dynamic loads on silos, especially shock and blast loads. The aim of this research is to evaluate the structural response of grain silos due to massive blast loads. The Beirut explosion that occurred on August 04, 2020 is considered as a case study in a structural engineering approach with numerical non-linear finite element modeling of the silos. Due to the uncertainty of the exploded material mass, the magnitude of the explosion is defined as the numerical model magnitude that generates the same silos damages and sways recorded on site. The numerical study models are based on silos data (geometrical and material properties), and the use of the Conventional Weapons Effects Blast Loading (CONWEP), and the Coupled Eulerian-Lagrangian (CEL) methods to generate the blast loads. In addition, damage for the standing silos has been assessed, and final recommendations were stated. The results of this study define the magnitude of the explosion and the structural state of the remaining silos.

Keywords: Blast Load, Beirut Explosion, Grain Silos, Nonlinear Analysis, Structural Damage, Dynamic Analysis, CONWEP, CEL, Clearing Effect.

1. Introduction

In recent times, explosion incidents have increased in different parts of the world, threatening lives and causing serious damages to infrastructures. The latter attracted the attention of several researchers in the field of structural engineering to study the effect of explosions and impact loadings on various structural elements [1-12].

Zhang [5] conducted a study on the effect of closed-in blast loads on RC beams. Eight beams were considered in this study, each was subjected to a blast resulting from different combinations of explosive weight and standoff-distance. Results showed that the mode of failure of beams subjected to closed-in blast is flexural due to plastic hinge formation. Temsah and Jahami [1-3] used the experimental data from Zhang [5] to apply a numerical analysis to study the effect of closed-in blasts on reinforced concrete (RC) beams. The numerical analysis accurately predicted the beam response to blasts, with results matching those obtained from experiments.

Within the same research work [1-3], additional investigation was conducted on the performance of reinforced concrete beams strengthened with carbon fiber reinforced polymer (CFRP) under blast loads. Research outcomes

included the derivation of Iso-damage curves for each beam, which showed the required pressure and impulse values necessary to trigger a certain level of damage. The research work proved the significance of certain considerations, mainly mechanical and dynamic material properties, in accurately forecasting through numerical analysis, the structural response and the excessive magnified equivalent static loads of the blast.

Anas [13] conducted a state of art review on the effect of blast loading on RC slabs as well as the methods of repairing, based on both experimental and numerical investigations. Several conclusions were derived from this review. It was proven that using CFRP sheets on the front face of slabs increases its blast load resistance. In addition, using Steel/Polypropylene fibers in concrete reduces damaged areas in both front and rear slab faces. As for slab deflection response, the authors recommended the use of steel plates with shear studs, or the installation of Aluminum foams on the slab front face acting as a shock absorber. These findings are important for additional research on RC slabs' response to blast loading. Similar findings were concluded by other studies addressing the methods of repairing of RC slabs damaged by blast loading [14-17].

Yan [18] studied the effect of blast loads on CFRP strengthened columns using both numerical and experimental analyses. It was proven that using CFRP increases the blast performance of columns and reduces the damage of concrete parts. Moreover, increasing the thickness of CFRP sheets improves column ductility. Another study by Lee [19] revealed that using ultra-high-performance fiber-reinforced concrete (UHPFRC) jacketing creates an adequate method to increase the blast performance of columns. Similar findings on the same topic were addressed by other researchers [20-21]. It is observed that all previous experimental research work was performed on reduced scale structural elements and non was conducted on realistic large scale complex structures. In addition, the performed numerical analyses of complex structures were not validated by field explosions results.

Many researchers examined collapsed silos to define the failure causes, and prevent similar future accidents [22-27]. These studies focused on structural assessment of silos using both finite elements and code provisions. However, the loads considered in these studies were static and temperature loads; dynamic and impact loads were rarely considered.

On August 04, 2020, a massive explosion took place at Beirut port. The explosive amount initially claimed to exist at the port was 2750t of Ammonium Nitrate. This explosion had incurred extensive damages in the surrounding areas, and was classified among the strongest in history. The grain silos, located in the port, in the vicinity of the warehouse where the explosion occurred, were said to have protected part of the city and its people from the blast. Recent studies were conducted to define the exploded quantity of Ammonium nitrate (AN). Some were physics-based studies such as the ones conducted by Rigby [28] and Dewey [29]; while others were based on blast damage assessment and seismic signals as Herbert [30] and Lewis [31]. All Conclusions emphasized that the explosive mass is less than the stored 2750 t of AN.

This research aims to investigate, through the analysis of the grain silos response to the blast, several explosion-related parameters such as the weight of the explosive mass, the role of the silos, and the soil effect. The proposed investigation method is based on non-linear finite element numerical analysis considering the exact dimensions of the silos, determined from existing structural execution drawings, and material properties obtained from site-collected specimen (concrete cylinders and reinforcing rebar), as well as blast loads generated from the conventional weapons (CONWEP) and the coupled Eulerian – Lagrangian (CEL) methods. The field structural damages, structure movement, and the crater size resulting from the explosion established validation criteria of the numerical analysis results. This study will help structural designers better understand the behavior of RC silos when subjected to blast loads.

2. Methods

Beirut grain silos (Figure 1) were built at Beirut port in the late 1960s and were inaugurated in 1970. They could store about 120,000 tons of grains, and their structure consisted of 42 cylinders, with an internal diameter of 8.5 m for each cylinder, walls thickness of 17 cm, and a height of 48 m. Over the years, expansion and rehabilitation works were executed. In the late 1990s, six new silos were added to the main 42 silos. In 2002, silos had undergone restoration works due to concrete carbonization [32].

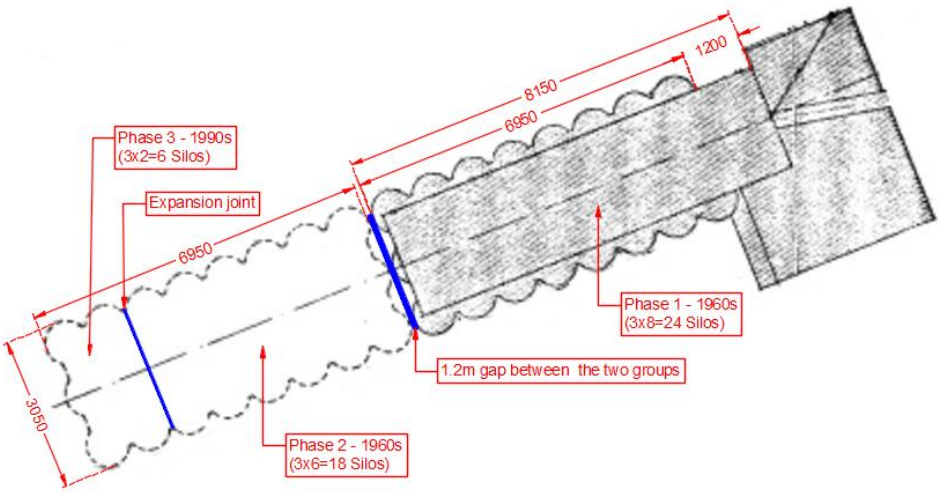

(a)

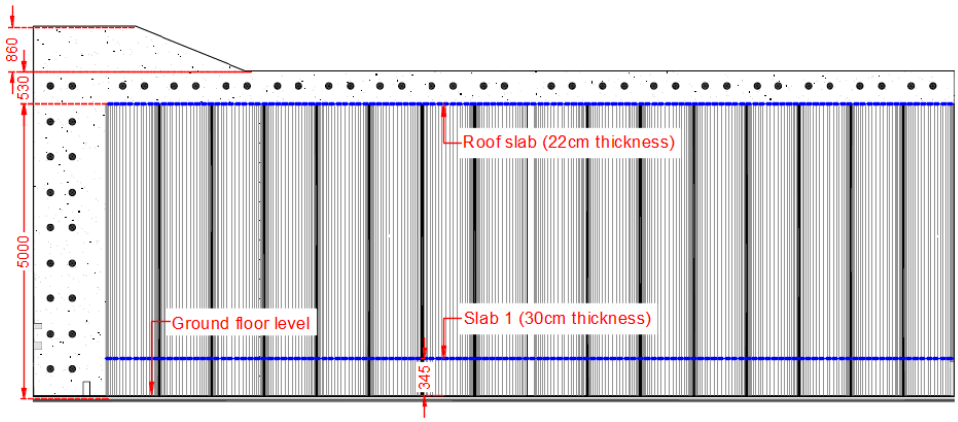

(b)

Figure 1:

(a) Planar dimensions for the grain silos (cm)

(b) Elevation dimensions for the grain silos (cm)

2.1 Geometry and Reinforcement

2.1.1 Original Design

The silos construction process was executed in three stages. First and second stages took place in the late sixties of the last century. The first phase included the construction of 3 rows of silos, with 8 silos in each row, i.e., a total of 24 silos. In the second stage, 3 rows of silos were added as an extension to the exiting 3 rows, each including 6 silos, i.e., a total of 18 silos were added. The silos of the second phase were 1.2 m spaced from the first phase silos. Thus, the total number of constructed silos by the end of stage 2 was 42. In the late nineties of the last century, two rows of silos were added, each row consisting of 3 silos, resulting in 6 new silos and increasing the total number to 48. Figure 1 shows the details of planar and elevation dimensions of the silos. Moreover, it shows the existence of two slabs at different levels, the first had a thickness of 30 cm at 3.45 m height from ground level, while the second slab (Roof slab) was 22 cm thick at the top of the silos, at 50 m height.

Figure 2 illustrates the internal layout of the silos. It can be noted that silos were connected in both longitudinal and transversal directions by stiffeners. The Longitudinal Stiffeners (LS) connected the silos along the transversal direction, and were spaced at 4.4 m. LS were 17 cm thick, extended from the level of Slab 1 to the level of Roof slab. Their dimensions changed due to the existence of a corridor on the ground floor as shown in Figure 3. In addition to the longitudinal stiffeners, 3.0 m long Transversal Stiffeners (T.S) connected the silos along the longitudinal direction, and their thickness varied from 17 cm in the middle zone to 52.5 cm at the edge zones. These stiffeners extended from the ground level to the roof slab level.

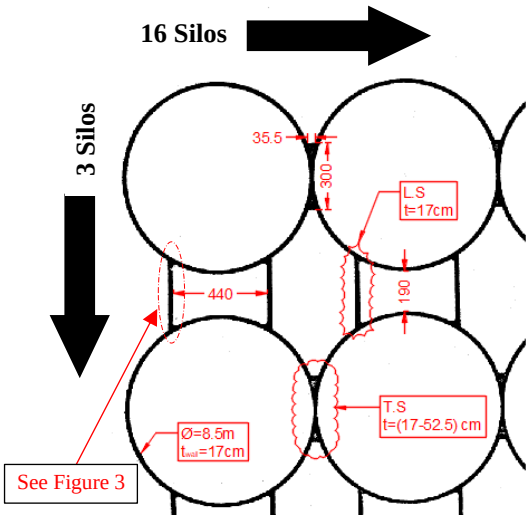

Figure 2: Internal division of silos (cm)

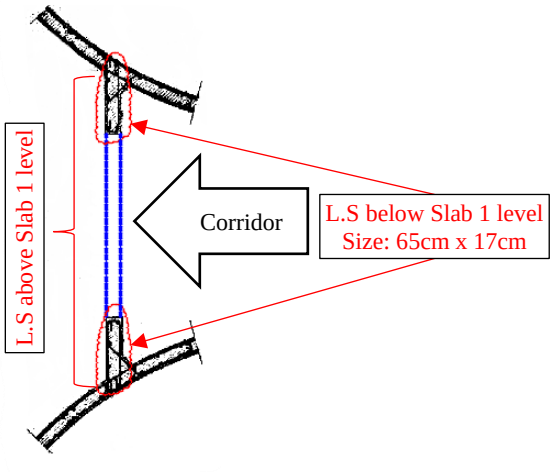

Figure 3: L.S dimensions below and above Slab 1 level (cm)

The silos reinforcing rebar and their distribution in the different concrete elements were determined from the original execution drawings as shown in Figures 4 and 5.

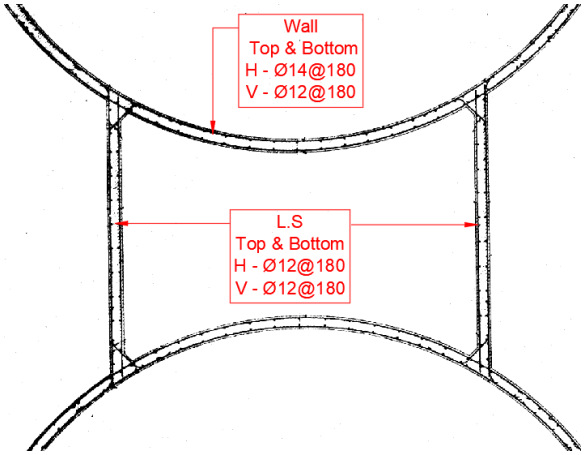

Figure 4: Walls and L.S reinforcement (mm)

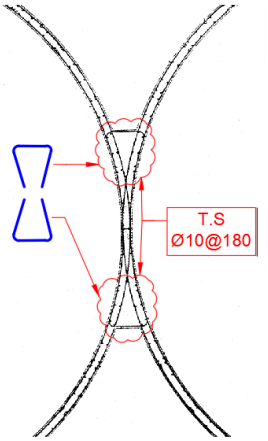

Figure 5: T.S reinforcement (mm)

2.1.2 Rehabilitation of Silos

From the years 2000 to 2002, the silos underwent rehabilitation works due to concrete deterioration in the two external silos long rows. The operation included the rehabilitation of the external 32 silos (first and third rows). The internal surfaces of the external rows were sand blasted and roughened using scabblers and bush hammers. Reinforcement details are shown in Figure 6.

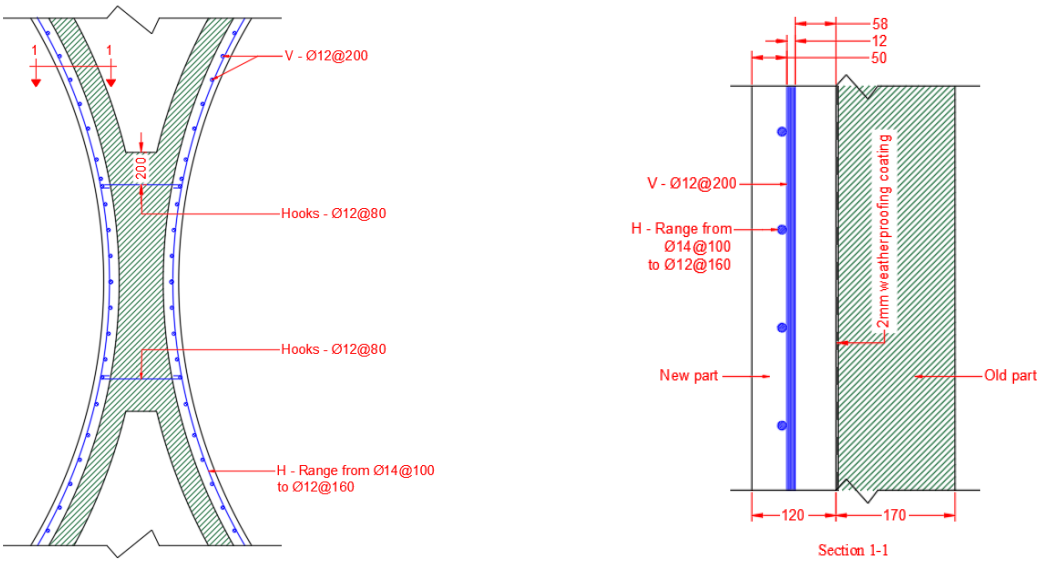

(a) (b)

Figure 6: a) Silos walls' reinforcement after rehabilitation (mm) b) Section 1-1 for the silo's wall (mm)

2.2 Material Properties

Concrete properties of silos were determined from experimental procedures. Site visits were conducted to extract concrete cores for material testing as shown in Figure 7. Ten cores (67 mm x 135 mm) were considered in this study; compressive strength tests were applied to five cores (specimens C1 to C5) (Figure 7), while splitting tensile tests were applied to the other five (specimens C6 to C10). The compressive tests were conducted in accordance to ASTM C42 requirements [33], while the splitting tensile tests were conducted in accordance to ASTM C496 [34]. Average compressive strength was correlated as per ASTM requirements, leading to 15.8 MPa (Figure 8a). The splitting tensile test results (Figure 8b) showed that the average tensile strength of concrete is 3 MPa. Table 1 summarizes concrete test results for all specimens. The density for each specimen was determined as shown in Table 1, the average density is 2350 kg/m^3. This value with the average compressive strength were used to determine the concrete modulus of elasticity following the ACI 318-14 Equation [35]:

$$E_c = 0.043 \times w_c^{1.5} \times \sqrt{f'_c} \quad (1)$$

Where "E_{co}" is the modulus of elasticity of concrete (MPa), "w_k" is the concrete density (kg/m^3), and "fe_{ck}" is the concrete compressive strength (MPa). Figure 9 show the concrete cores after compression and splitting tensile tests.

Figure 7: Concrete coring & Core testing

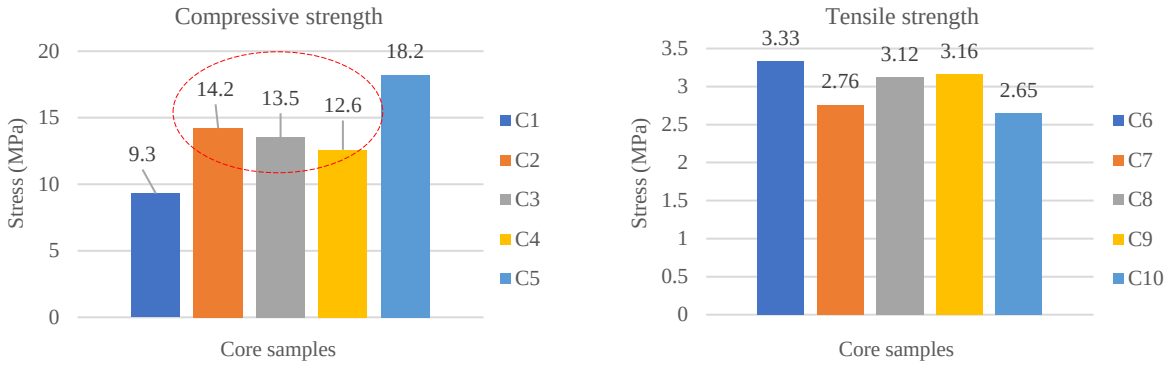

(a) (b)

Figure 8: a) Compression test results b) Splitting tensile test results

Table 1: Concrete specimens test results

Sample	Mass (kg)	d^a (mm)	L^{ob} (mm)	V^c (mm^3)	ρ^d (kg/m^3)	$(f'_c{}^e)$ or $(f_t{}^f)$ (MPa)	Correlated strength (MPa)	E^g (MPa)
C1	1.1	67.0	134.0	472197.9	2316.8	9.3		
C2	1.1	67.0	134.0	472197.9	2261.8	14.2		
C3	1.1	67.0	134.5	473959.8	2323.0	13.5	15.8	
C4	1.1	67.0	135.0	475721.8	2396.4	12.6		
C5	1.2	67.0	138.0	486293.4	2383.3	18.2		19467
C6	1.1	67.0	128.5	452816.7	2336.5	3.3		
C7	1.2	67.0	135.0	475721.8	2423.7	2.8		
C8	1.1	67.0	127.0	447530.9	2446.8	3.1	3.0	
C9	1.1	67.0	135.0	475721.8	2312.3	3.2		
C10	1.1	67.0	135.0	475721.8	2289.2	2.7		

a: Core diameter, b: core length, c: core volume, d: concrete density, e: compressive strength, f: tensile strength, g: Elasticity modulus

(a) (b)

Figure 9: a) Concrete cores after compression test b) Concrete cores after splitting tensile test

Similar to concrete specimen, several steel rebar specimens were sampled for uniaxial tensile test according to ASTM A615 [36] requirements (Figure 10). For each size, two specimen categories were considered; specimens from the old silos' parts (before rehabilitation), and specimens from the new parts (after rehabilitation). Two specimens were considered for each size to obtain average yield strength after testing (Figure 10). Test results are summarized in Figure 11. The average yield strength for:

- Rebar 10 mm diameter, of the new part is 522 MPa, and 407 MPa for rebar from old parts.
- Rebar 12 mm diameter, of the new part is 447 MPa, and 505 MPa for rebar from old parts.
- Rebar 14 mm diameter, of the new part is 464 MPa, and 455 MPa for rebar from old parts.

Figure 10: Uniaxial tensile test for rebars

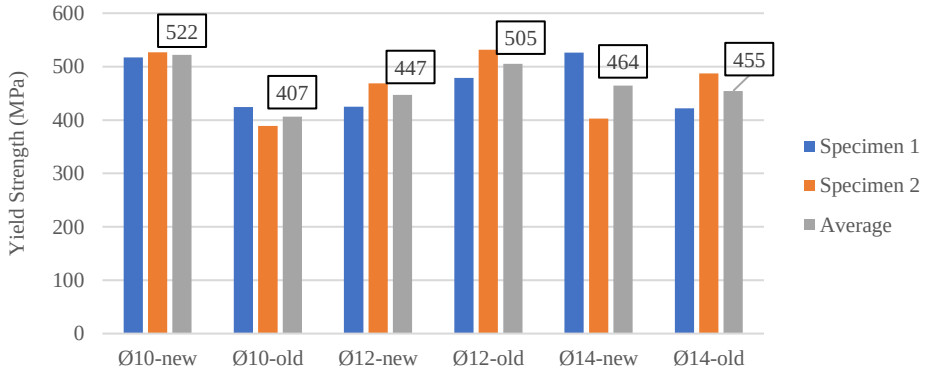

Figure 11: Tensile test results for all rebar specimens

The soil investigation was performed with 2.0 m depth pit at vicinity of silos building. The pits revealed 3 soil layers at 40 cm, 50 cm, and a final deep layer. Several samples were extracted from each layer and subjected to laboratory tests (Figure 12) to define their properties; namely: density, elasticity modulus, Poisson's ratio, angle of friction and cohesion. Results of the deep soil layer led to a density of 1864 kg/m^3, an elasticity modulus of 20 MPa, a Poisson's ratio of 0.3, and an angle of friction of 35°. However, no cohesion stress was recorded for the soil since it is a sandy soil.

Figure 12: Soil profile, specimens, and laboratory tests

2.3 Damage and Sway Assessment

The research team conducted several field visits to assess the damages of the silos. In addition, several high-resolution aerial photos of the silos were captured, as shown in Figure 13. It can be concluded from the site observations and the aerial photos that the first row of silos is completely destroyed, as well as most of the second row. It is also noticed that the last two silos of each row (the first, second, and third) are completely destroyed, as shown in Figure 13. Figure 13c shows the front view of the silos, where some parts of the second-row silos are suspended from the third row. Only 14 silos of the third row are still standing after the explosion as shown in Figure 13. In addition to the silos' damages, the size of the crater that resulted from the explosion was used as a validation parameter for the numerical model. The crater is elliptical in shape with larger and shorter diameters of 106 m and 90 m.

(a)

(b) (c)

Figure 13: a) Aerial photo for silos after the explosion b) Side view for the damaged silos c) Front view for the damaged silos

A site three-dimensional scanning for the silos was performed [37] showing the deformed shape of the remaining part (14 silos of the third row) as illustrated in Figure 14. The scanning showed that the silos exhibit maximum lateral sway of 30 cm, along with the direction of the blast. It also showed that the inner half of the remaining third silos row is severely damaged, and therefore is not structurally safe.

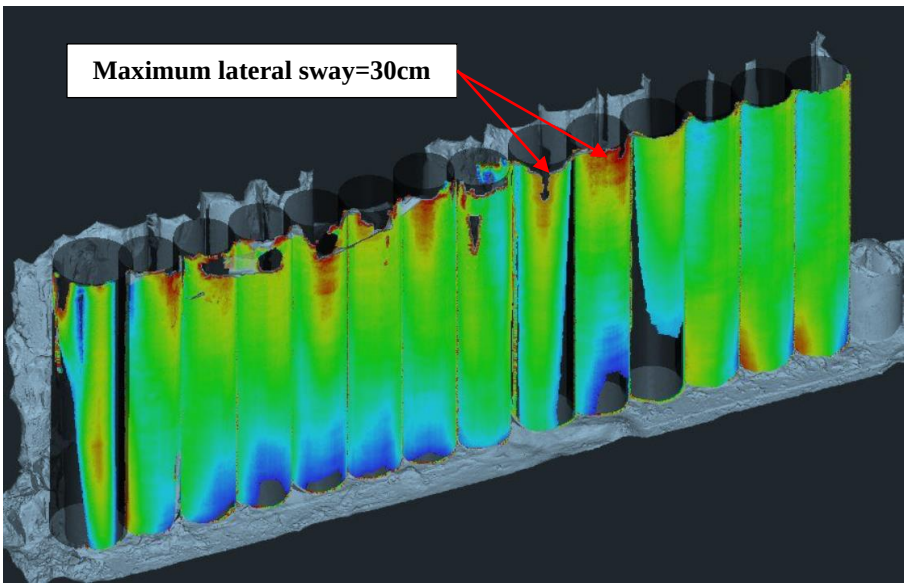

Figure 14: 3D scan done for remaining silos [37]

3. Numerical Modeling

3.1 Finite Element Model

After collecting all the information related to the silos, a non-linear numerical analysis was conducted using ABAQUS software, to determine the structural response of silos building based on damage levels and maximum displacement. Four-node doubly curved thin shell elements were used to model the silos walls, as shown in Figure 15. Longitudinal stiffeners (L.S), transversal stiffeners (T.S), and slabs were modeled using the built-in shell elements, as illustrated in Figures 15b and 15c. The reinforcing rebar are represented by layers embedded in the shell elements. Several layers of reinforcement (rebar) are assigned to each shell element, by specifying a unique name for each layer, selecting the material constituting each layer, and specifying the cross-sectional area per rebar, spacing, and orientation of the rebar in each layer. The filling grains are modeled with 8-node linear brick elements, and placed inside the silos. Based on the data collected from different sources and field visits, all silos were filled with grains, except for the last two silos of each row (Figure 13a). Similarly, the supporting soil medium was modeled with 8-node linear brick elements, considering 20 m depth underneath the silos building.

Regarding meshing of elements, a mesh size of 1.5 m was used for all silos' structural components (shell and brick elements) and grains' elements. This size was chosen after several iterations to reach the best mesh size that leads to high accuracy in the analysis. As for the Eulerian domain adopted in the CEL model, a mesh size of 3 m was chosen based on mesh sensitivity analysis that is further presented within the results paragraph. The Eulerian domain dimensions are 150 m parallel to the blast wave direction, 450 m in the direction parallel to the silos' length, and 300 m parallel to the silos' height. These dimensions were defined further to several numerical analysis iterations reduce the run-time without affecting the accuracy of the results.

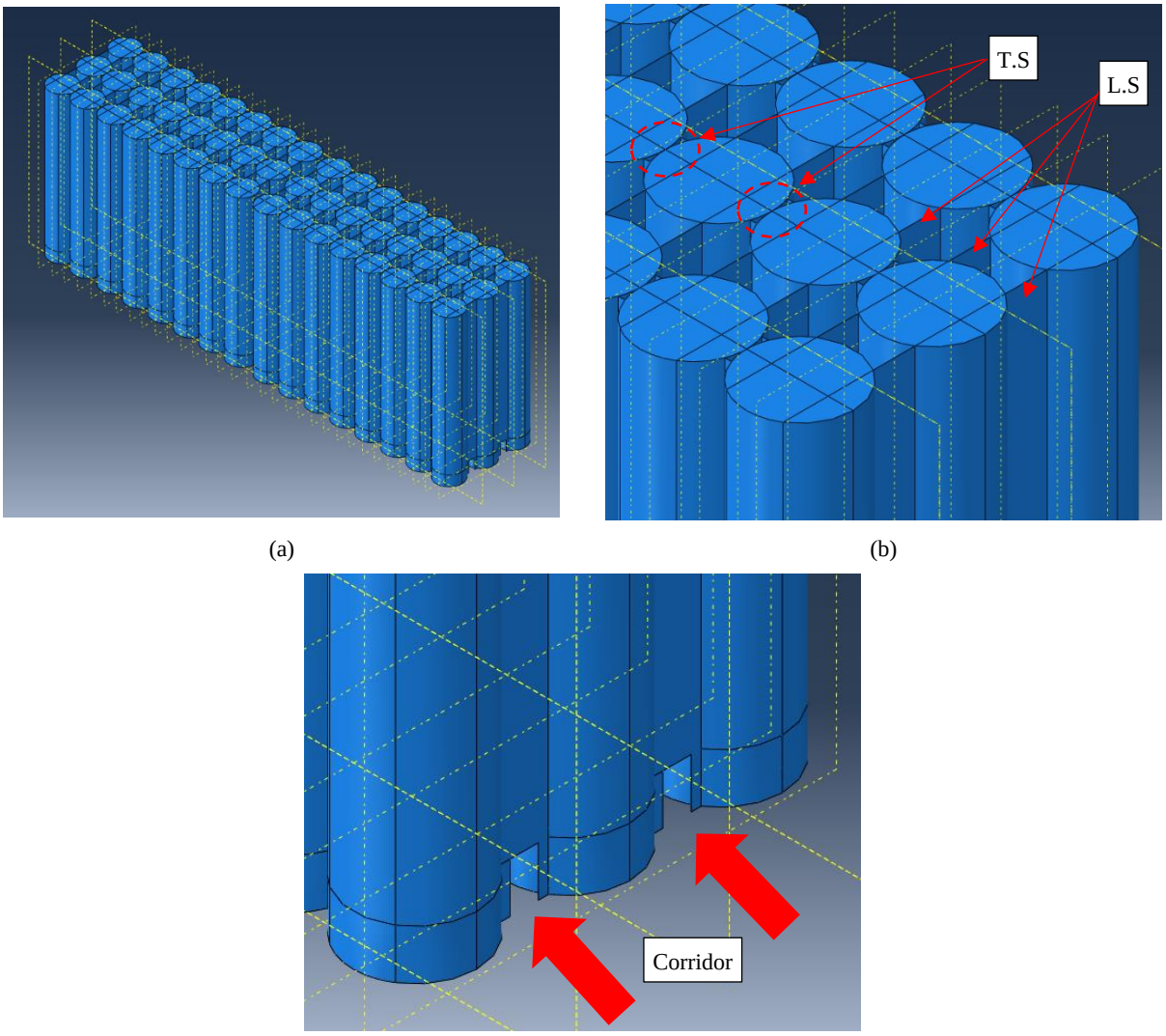

(a) (b)

(c)

Figure 15: a) 3D view for the finite element model for silos b) 3D view showing L.S and T.S c) L.S below the first floor where there is a corridor

3.2 Material Definition

The built-in Concrete Damage Plasticity model (CDP) was used to model the mechanical properties of concrete. This method is highly efficient when studying concrete under dynamic and impulsive loads. CDP model considers the nonlinear behavior of concrete by defining different input parameters such as inelastic strain, cracking strain, stiffness degradation and recovery, as well as other parameters. In addition, strain rate effect on concrete mechanical properties was considered by adopting CEB-FIP Model relations [38]. The authors determined the value of the strain rate by successive iterations [1, 39]. The first analysis iteration was performed considering the static properties of the material. Based on the strain rate resulting from the analysis, the material properties were updated. Additional iterations were performed until the convergence of the strain rate values. CDP model is used by many researchers to accurately define the concrete mechanical properties under dynamic load conditions [1-4]. Table 2 shows CDP parameters used in the analysis.

Table 2: CDP parameters used in modeling [1-4]

Parameter		Concrete of original silos	Concrete rehabilitated silos
Elastic Modulus (MPa)	E	19467	22800
Poisson's ratio	υ	0.2	0.2
Density (Kg/m^3)	ρ	2400	2400
Compressive strength (MPa)	fa_{ct}	15.8	23.7
Peak Compressive strain (mm/m)	a_{ce}	1.06	1.13
Tensile Strength (MPa)	f_t	3	3
Strain rate (s^{-1})	$\dot{\epsilon}$	0.24 - 4	0.24 - 4
Dilation angle (^{0})	ψ	36	36
Eccentricity	ε	0.1	0.1
Bi-axial to Uni-axial strength ratio	f_{b0}/f_{t0}	1.16	1.16
Second stress invariant ratio	K	0.67	0.67
Viscosity parameter	μ	0	0

Regarding steel material for rebar, the elastoplastic behavior is adopted in this study. This leads to steel material behaving elastically up to the yield point. After yielding, it behaves perfectly plastic. Yield is determined from the lab experiments discussed earlier. Grains are modeled as granular material using the Mohr – Coulomb method. This method determines the combination of axial and shear forces that cause the material to fail. Many researchers investigated the grain properties and determined Mohr – Coulomb parameters for grain materials, which are: the density (769 kg/m^3) [40], the modulus of elasticity (18 MPa) [41], the angle of friction (30°) [42], and the cohesion stress which has the value of zero for granular materials. Abaqus built-in "Contact" is defined and assigned for all grain-concrete surfaces with both "hard" and "tangential" contacts. The model consists of 3 parts separated by expansion joints as shown in Figure 16. The soil medium was modeled similarly to the grains since the soil underneath silos is granular; the Mohr – Coulomb criteria is based on the properties resulting from the experimental laboratory tests (section 2.2). Regarding the contact between the Eulerian domain (air and soil) and the silos, Abaqus built-in "General Contact" is defined. This contact automatically computes and tracks the interface between the Lagrangian structure and the Eulerian material to ensure the two domains (Eulerian and Lagrangian) do not occupy the same physical space.

The Jones-Wilkins-Lee (JWL) equation is used to define TNT explosive properties [43], while the air is modeled as an ideal gas, as shown in Table 3. The latter specifies all required parameters to define TNT explosives and air medium properties.

Table 3: JWL parameters for TNT and Air properties [43]

	TNT (JWL model)	AIR (Ideal Gas)	Units
Mass density	1630	1.293	Kg/m^3
Detonation wave speed	6930	-	m/s
A	$3.738x10^{11}$	-	Pa
B	$3.747x10^{9}$	-	Pa
R_1	4.15	-	-
R_2	0.9	-	-
ω	0.35	-	-
Specific Energy	$3.68x10^{6}$	-	J/kg
Ambient Pressure	101325	101325	N/m^2
Specific Gas Constant	-	286.9	J/kg.K
Specific Heat	-	717	J/kg.K
Viscosity	-	$1.82x10^{5}$	kg/m.s

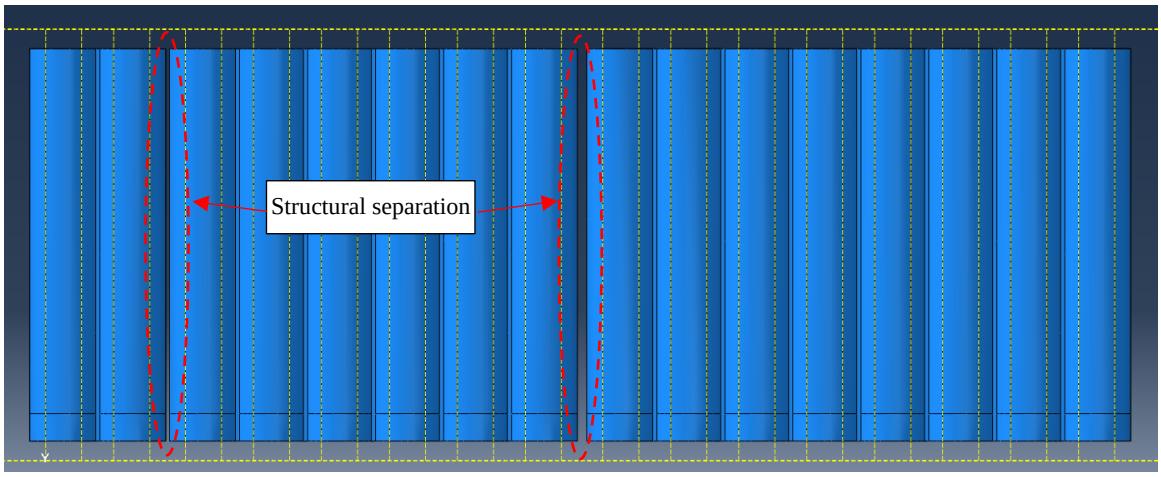

Figure 16: Structural separations where the surface-to-surface contact assigned.

3.3 Blast Load Definition & Work Plan

ABAQUS built-in CONWEP and the Coupled Eulerian – Lagrangian (CEL) methods are respectively used to generate the blast load. The CONWEP model simulates the loading effects due to spherical air blasts and hemispherical incident surface blasts, in terms of both incident and reflected pressures [44]. The typical pressure history for a blast wave is shown in Figure 17. Based on this method, the total pressure applied on the front surface is defined as:

$$P(t) = P_i(t)[1 + \cos\theta - 2\cos^2\theta] + P_r(t)\cos^2\theta \quad , \text{for } \cos\theta > 0 \qquad (2)$$

$$P(t) = P_i(t) \quad , \text{for } \cos\theta < 0 \qquad (3)$$

Where "P(t)" is the total surface pressure at time t, "P_i" is the incident pressure, and "P_r" is the reflected pressure.

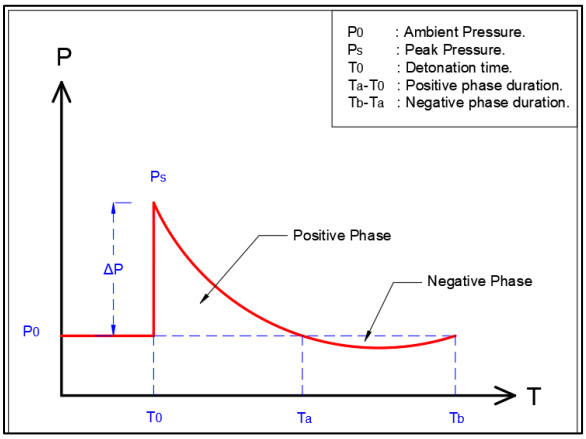

Figure 17: Typical pressure history for a blast wave

The CEL method is commonly used when the interaction between the fluid (air) and structures is to be solved simultaneously. It enables the user to mesh the analysis components undergoing large deformations using Eulerian technique while the remaining parts using the conventional Lagrangian technique. The interaction behavior between the two techniques is modelled by "General Contact" definition. The advantage of the CEL method compared to the (CONWEP) is that it accurately considers the blast wave– ground interaction, which leads to a magnification in the blast pressure values. However, the run time using the CEL method is relatively higher than that using the CONWEP method. Based on preliminary location of the center of explosion, the CONWEP was used as a first phase of analysis to determine the exact location of the center of explosion and the magnitude of the explosion. The CEL is used to determinate the magnitude of the explosion considering the same explosion location as derived from the first phase.

In Beirut blast case, the blast is surface type since it took place at ground level. The aerial photos of silos were used to define the preliminary detonation center point as shown in Figure 18. The figure shows also warehouse 12 that contained the explosive materials, the silos, structures behind the silos, and the crater resulted from the explosion. Based on the apparent crater extent, the preliminary center point of explosion was determined by considering the center of crater, which lies 75m away from silos front face. The center of explosion was adjusted based on model calibration requirements.

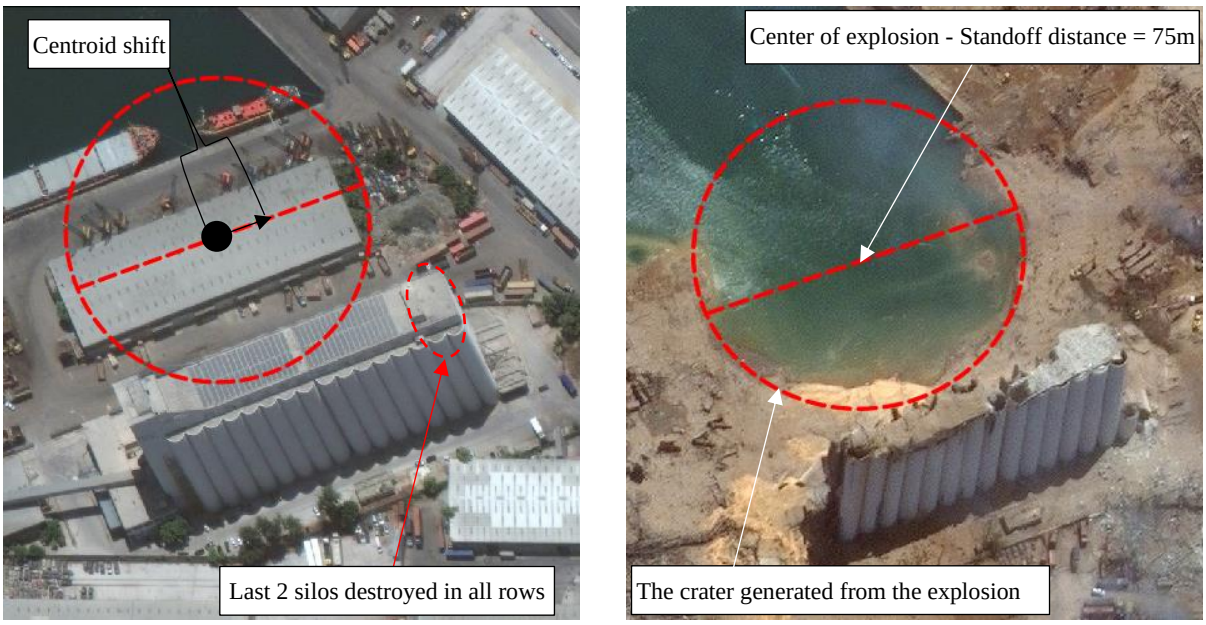

(a) (b)

Figure 18: a) Silos' vicinity before explosion b) Silos vicinity after explosion

Since the explosive material in warehouse 12 is Ammonium Nitrate (AN), a scaling factor is used to transform the AN mass to equivalent TNT mass [45], to enable using it in the numerical study as an input. The following Equation is adopted for this purpose:

$$W_e = \frac{H^d_{exp}}{H^d_{TNT}} W_{exp} \quad (4)$$

Where *"W_e"* is the equivalent TNT charge weight (kg), *"W_{exp}"* is the weight of the explosive (kg), *"H^d_{exp}"* is the heat of detonation of explosive (J/kg), and *"H^d_{TNT}"* is the heat of detonation of TNT (J/kg). The heat detonation of TNT ranges between 4.1 MJ/kg - 4.55 MJ/kg while the detonation heat of AN is 1.59 MJ/kg. According to equation 4, the scaling factor ($\frac{H^d_{exp}}{H^d_{TNT}}$) ranges between 0.35 – 0.39 for AN to TNT transformation. Referring to the investigations on the stored AN, a scaling factor of 0.39 is recommended to transfer the explosive mass from AN to TNT. This implies that the total original mass of AN of 2750 t, is equivalent to 1100 t of TNT.

The phase 1 (CONWEP) includes 8 study cases with different values of explosive mass. Case 1 considers the detonation corresponding to 1100 t of TNT (equivalent to the whole original 2750 t of AN). The analysis started by case 1 to check if the original quantity generated the resultant damages. Cases 2 to 7 consider different detonation amounts of AN explosive (45%, 36%, 27%, 18%, 9% and 4.5% of the total 2750 t amount). Several parameters are considered to calibrate the model, the degree of damages for silos and structures behind as shown in Figure 13, the top lateral sways for the remaining third row of silos shown in Figure 14, and the crater size generated from the explosion (Figure 18). The last case (Case 8) was chosen based on the results of the previous seven runs, as the case that generates damages similar to the current damaged silos. In order to generate the total destruction of the last two

silos in all silos' rows, shifting of the centroid by 10 m towards the edge destroyed silos is needed, as illustrated in Figure 18.

4. Results and Discussion

4.1 CONWEP Method

Results of all study cases are summarized in Table 4 including damage level, maximum top displacement, blast wave pressure, maximum reactions, strain rate, and total external work. Figure 19 shows the damage pattern for all load cases. It is noted that for equivalent TNT mass of 1100 t, 500 t, 400 t, and 300 t respectively, all silos will be totally destroyed (cases 1 to 4), which does not represent the actual damage state considering the remaining silos. As for the cases with equivalent TNT mass of 200 t and 100 t, two out of three rows will be completely destroyed. Reducing the mass of explosion to 50 t results in destruction of just one row of silos as shown in Figure 19. Damage level results for cases 1 to 7 are illustrated in Figure 20.

Table 4: Summarized results for all study cases

Case	TNT (t)	d[a] (m)	Z[b] (m/kg$^{1/3}$)	Damage level[c]	δ_{max}[d] (cm)	P_s[e] (MPa)	$F_{base-max}$[f] (kN)	$M_{base-max}$[g] (kN.m)	$\dot{\varepsilon}$[h] (s^{-1})	W_t[i] (J)
Case 1	1100	75	0.727	3 rows	202	17.2	1846180	1818540	4	6.28 x 10^9
Case 2	500	75	0.945	3 rows	82	9.1	1121450	1113400	1.41	1.68 x 10^9
Case 3	400	75	1.018	3 rows	62	7.5	956968	940165	1.25	1.15 x 10^9
Case 4	300	75	1.120	3 rows	44	5.35	796972	744287	1.24	7.04 x 10^8
Case 5	200	75	1.282	2 rows	31	3.82	615301	523658	0.68	3.56 x 10^8
Case 6	100	75	1.615	2 rows	18	1.9	462448	288411	0.47	1.12 x 10^8
Case 7	50	75	2.036	1 row	10	0.95	380292	158076	0.24	3.6 x 10^7
Case 8[j]	210	75	1.261	2 rows	26	2.63	575718	451001	0.68	2.58 x 10^8

a: standoff distance, b: scaled distance, c: number of silos-rows destroyed from the explosion, d: maximum displacement in the direction of the applied blast load, e: peak blast pressure on silo's front surface, f: maximum reaction at base in the direction of the applied blast load, g: maximum moment reaction corresponding to the applied blast load, h: strain rate, i: Total work generated, j: detonation point was shifted by 10m towards the direction shown in Figure 18.

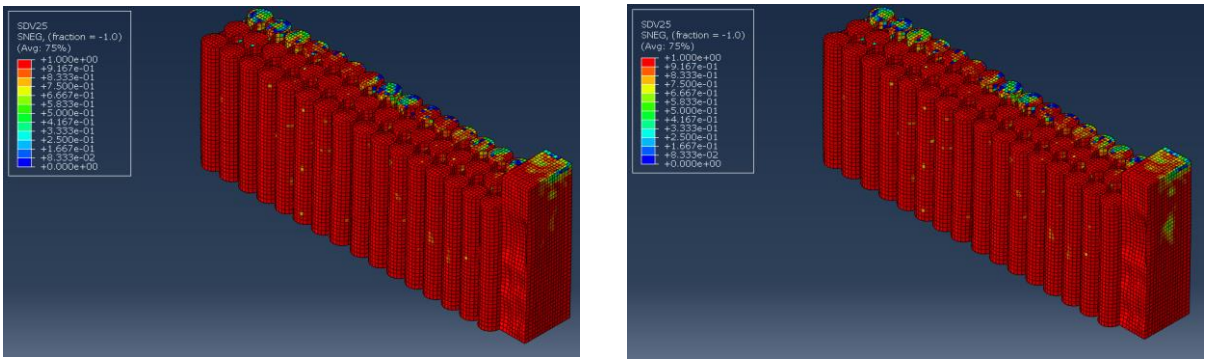

(a) (b)

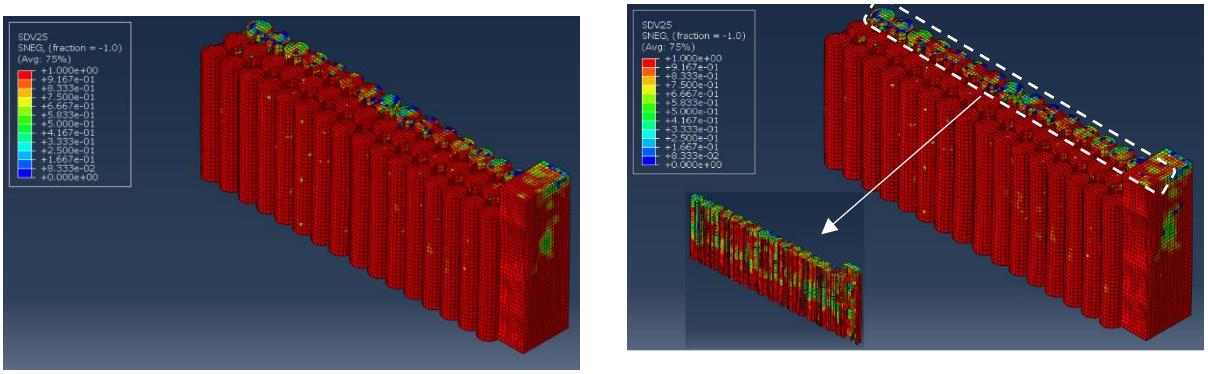

(c) (d)

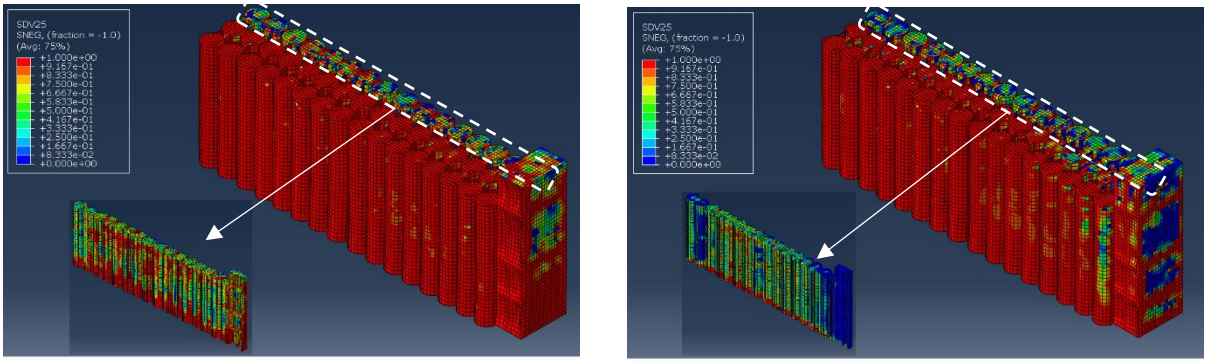

(e) (f)

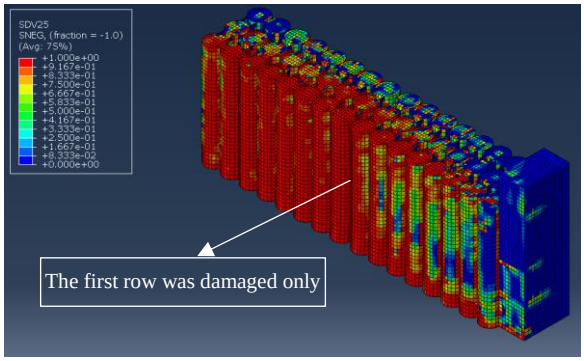

(g)

Figure 19: Damage pattern for study cases:

a) Case 1 b) Case 2 c) Case 3 d) Case 4 e) Case 5 f) Case 6 g) Case 7

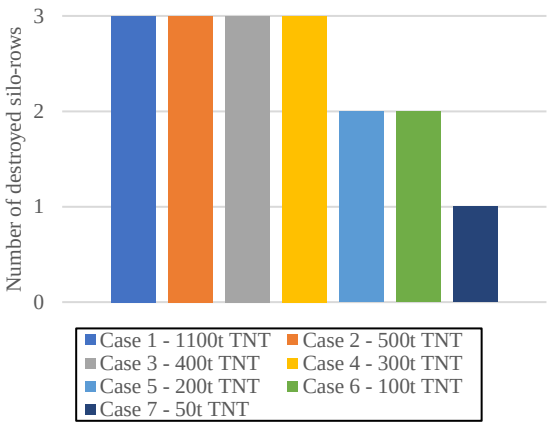

Figure 20: Damage level for cases 1 to 7

Regarding blast pressure, Figure 21 summarizes the peak pressure of the silos for each case study. For 1100 t of equivalent TNT explosion, the peak blast pressure is 17.2 MPa. This value decreases to 9.1 MPa, 7.5 MPa, and 5.35 MPa for 500 t, 400 t, and 300 t of equivalent TNT respectively. It is noted that a minimum peak pressure of 5.35 MPa is required to cause a total failure for all silos-rows based on the considered study cases. As for the remaining equivalent TNT masses, the peak blast pressure values are 3.82 MPa, 1.9 MPa, and 0.95 MPa for 200 t, 100 t, and 50 t respectively. This indicates that a peak blast pressure of 1.9 MPa is required to destroy 2 silos rows, whereas peak pressure values between 1.9 MPa and 0.95 MPa cause damages of one silos row only.

These applied peak pressures led to reaction forces and moments at silos base that had similar trend as the peak pressure (Figure 22). Reaction forces and moments ($8.0x10^5$ kN and $7.4x10^5$ kN.m) for case 4 are minimum reactions required to destroy all silos, while those for case 6 ($4.62x10^5$ kN and $2.9x10^5$ kN.m) are minimum reactions required to destroy 2 silos-rows. As for reaction values lower than the values of case 6, they destroy only one row of silos.

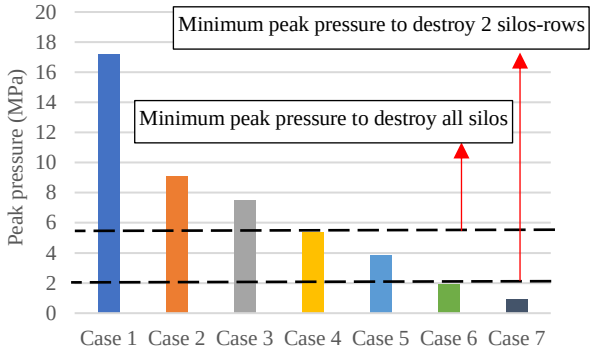

Figure 21: Peak pressure values for all case studies

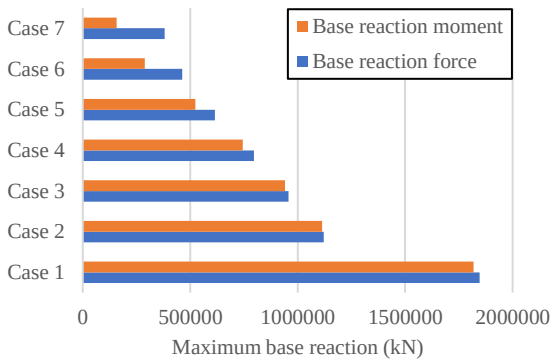

Figure 22: Reaction force and moment for all case studies

Moreover, the maximum lateral sways in the direction of blast pressure are shown in Figure 23. The sways have the same trend, similarly, the blast pressure and reactions. It is noted that cases 1 to 4 have maximum sway values, larger than the 30 cm value determined by the 3D scanning [37]. This given along with the damage level, emphasizes the adequate choice of a 200-t equivalent TNT blast magnitude at a 75 m standoff distance. However, location of this weight needs adjustment to provide the exact damage pattern.

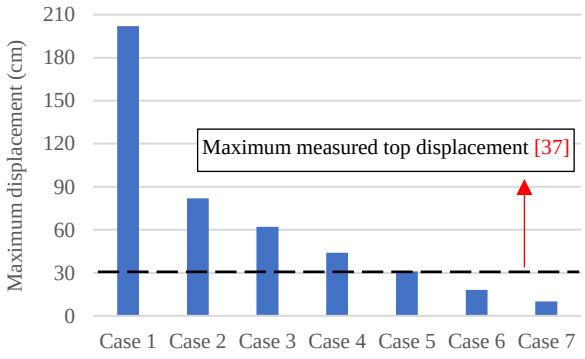

Figure 23: Maximum displacement for all study cases

Figure 24 shows the damage for silos in case 8, where the blast centroid is shifted by 10 m towards the side where the last two silos were totally destroyed, to provide results matching the damage level as the actual case. It is noted that the first and second rows are completely destroyed. However, the third-row experienced destruction in the last two silos as shown in Figure 24c. This matches exactly the damage pattern summarized in Figure 13. In addition, it was observed by the specialist who performed the site 3D scanning that the internal faces of the remaining silos are partially damaged. This is shown in Figure 24c where 3 of the remaining silos are excessively damaged at the front face. It is also worth mentioning that the damage at the base of the remaining silos may be overestimated due to the rigid boundary condition.

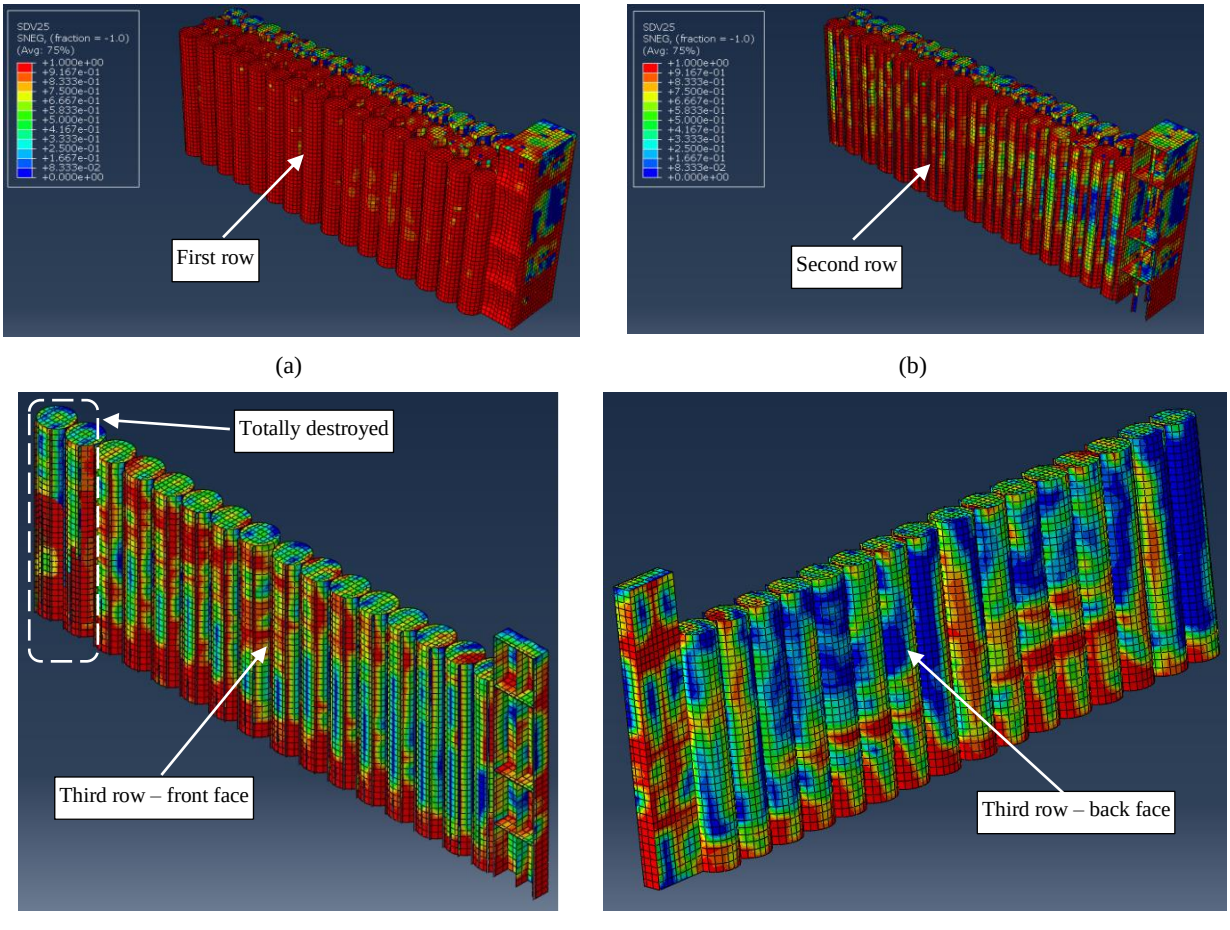

Figure 24: Damage pattern for case 8

a) First row b) Second row c) Third row – front face d) Third row – back face

As for the sway of the remaining silos in the direction of applied blast loading, the results show that the maximum sway is 27 cm (Figure 25). This value is detected in silo number 11 as shown in Figure 25b. According to this Figure, silos of the second phase (refer to Figure 1) are displaced more than silos from the first phase, since the center of blast loading is closer to the second phase, 10 m shifting of blast centroid. The maximum sway value is close to the value detected by 3D scanning which is 30 cm, indicating that the TNT mass is appropriate for this degree of sway.

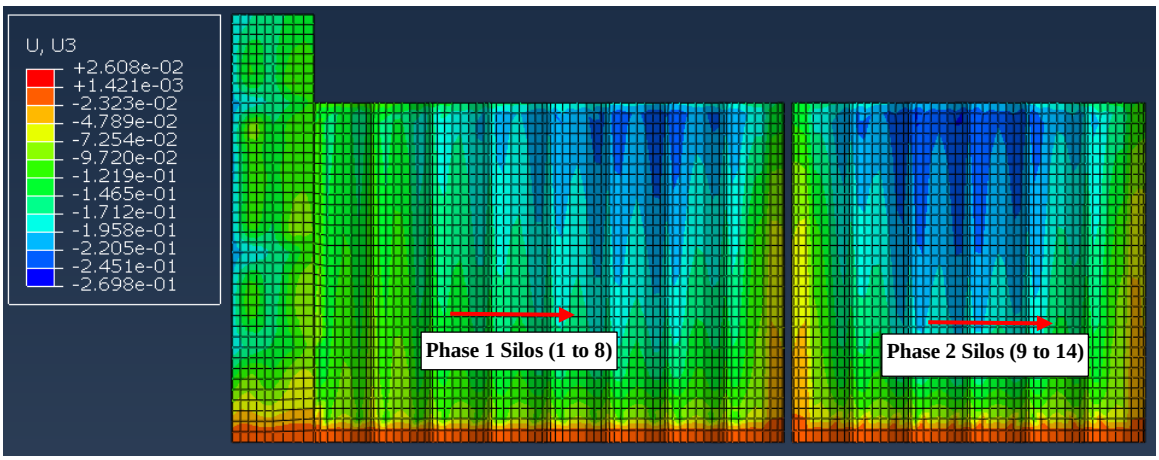

(a)

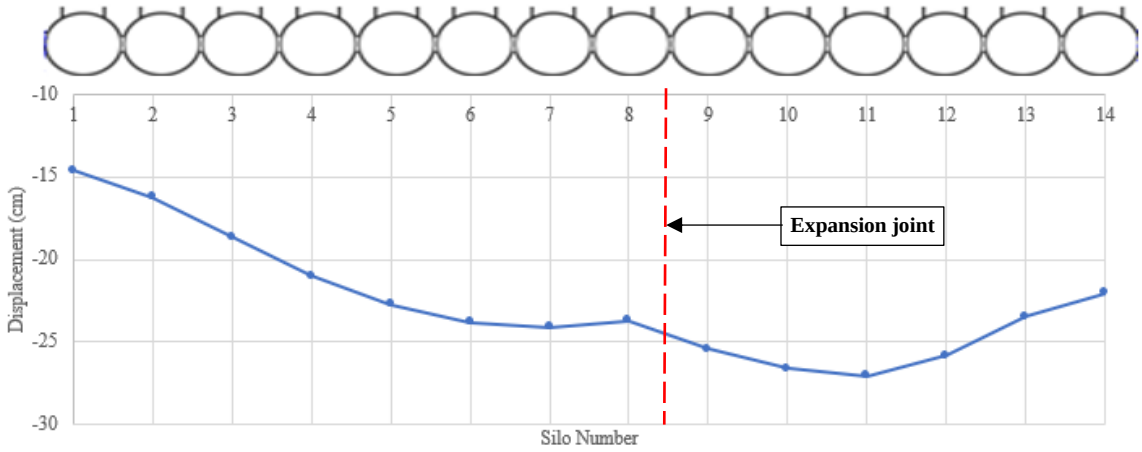

(b)

Figure 25: a) Displacement in the direction of blast b) Maximum displacement for each silo - CONWEP (cm)

4.2 CEL Method

Based on the magnitude and location obtained from CONWEP method, a second phase of numerical analysis was completed using the CEL method. The blast wave propagates with semi-spherical shape due to ground surface existence. The wave engulfed the silos at 400 ms after the blast took place as shown in Figure 26.

The CEL method concluded that the blast was a result of 220 t TNT explosive mass (equivalent to 564 t of AN). This mass was concluded by the calibration of the damage level in the remaining silos, the top maximum lateral sway, and the crater dimensions. The determined quantity of TNT from the numerical analysis is close to the quantities resulting from previous recent studies conducted by Dewey [29], Herbert [30], and Lewis [31] on Beirut explosion, which resulted in the average percentage of exploded equivalent TNT quantity as 27%, 23%, and 32% respectively. Figure 27 shows the damage level for the front and back faces of the remaining silos at the third row. Silos experienced a degree of damage matching the actual level detected on site (Figure 13). As for the maximum top displacement (sway), Figure 28 shows that the maximum lateral displacement is 29 cm and occurred at silo number 9.

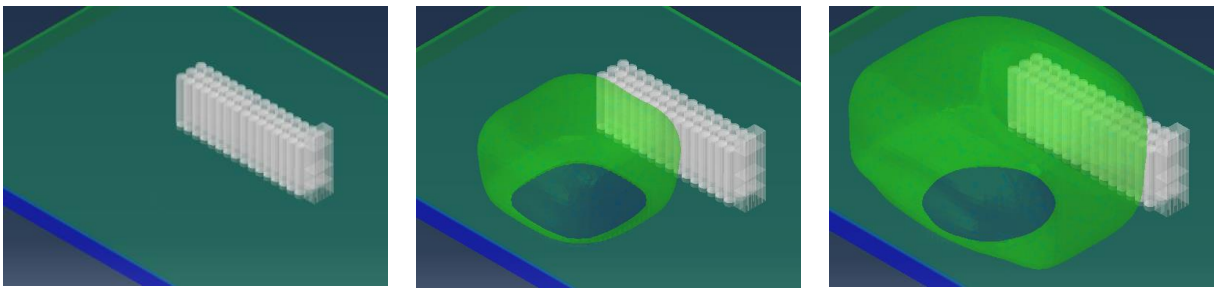

(a) (b) (c)

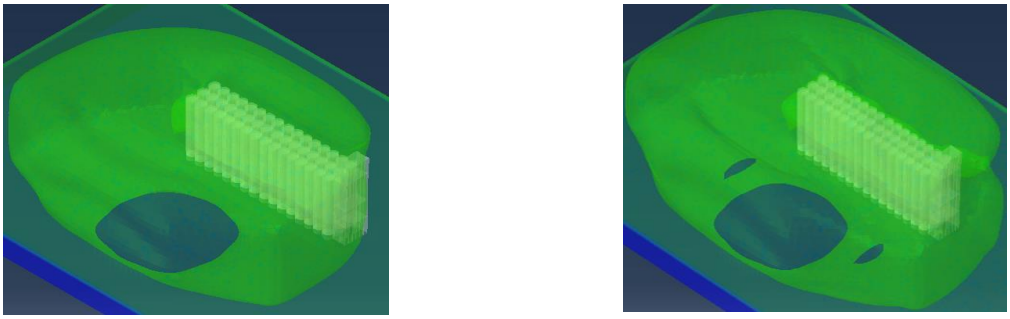

(d) (e)

Figure 26: Blast wave propagation at:

a) t=0 ms b) t=100 ms c) t=200 ms d) t=300 ms e) t=400 ms

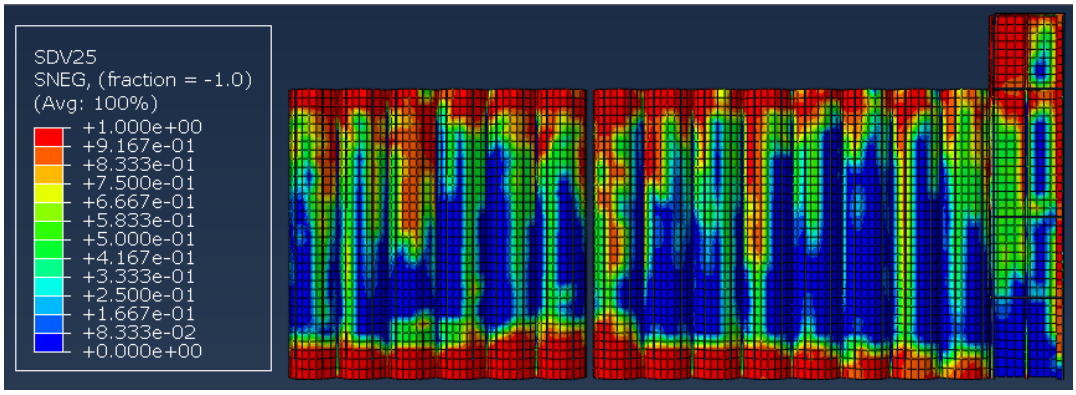

(a)

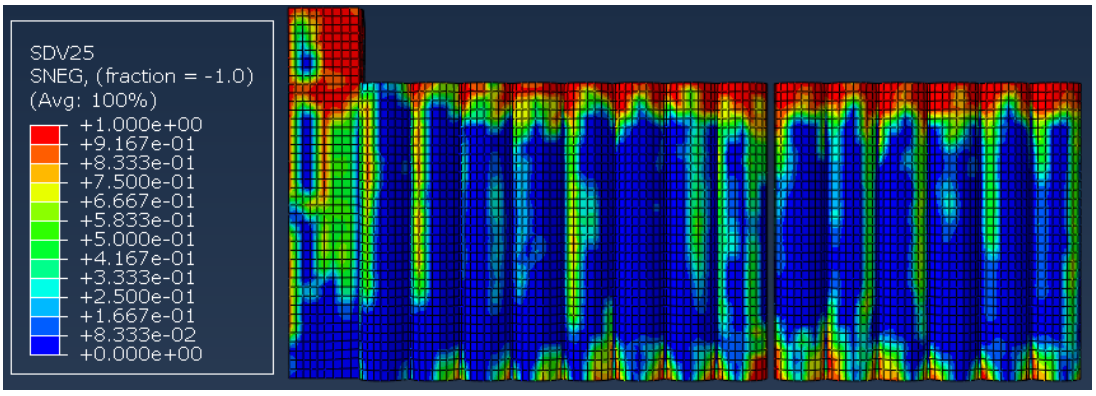

(b)

Figure 27: Damage layout of the remaining silos in the third row: a) Front face b) Back face

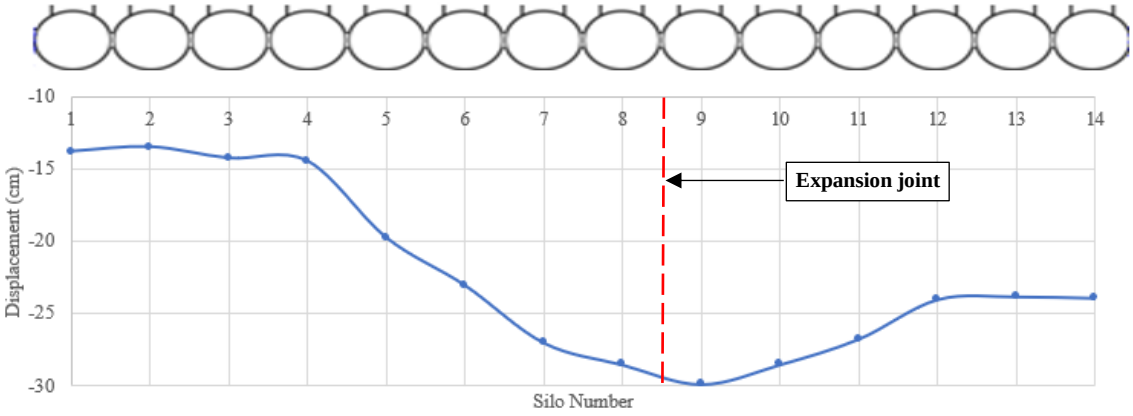

Figure 28: Maximum displacement for each silo – CEL method (cm)

The crater size that resulted from the explosion is used to validate the numerical model. Site measurements [46] showed that the formed crater has an elliptic shape of diameters 106 m x 90 m, while numerical analysis generated crater dimensions of 92 m x 86 m (Figure 29). The differences in crater dimensions between numerical analysis and the real dimensions are (13% x 4%). The crater dimensions from numerical analysis were determined from the plastic strain of soil. High plastic strain values indicate a soil collapse due to explosion.

Regarding the effect of shock waves on ground surface and the soil underneath silos, it was revealed that the impact of the explosion on the ground extended to cover the whole Eulerian domain considered in this study as shown in Figure 30. The results show that the peak soil pressure from the blast had a value of 60 MPa and covered a circular zone of 18 m radius measured from the center of explosion. As we move away from the explosion center, the soil pressure decreases until reaching a value of 0.3 MPa at a distance of 165 m (edge boundary of the Eulerian domain).

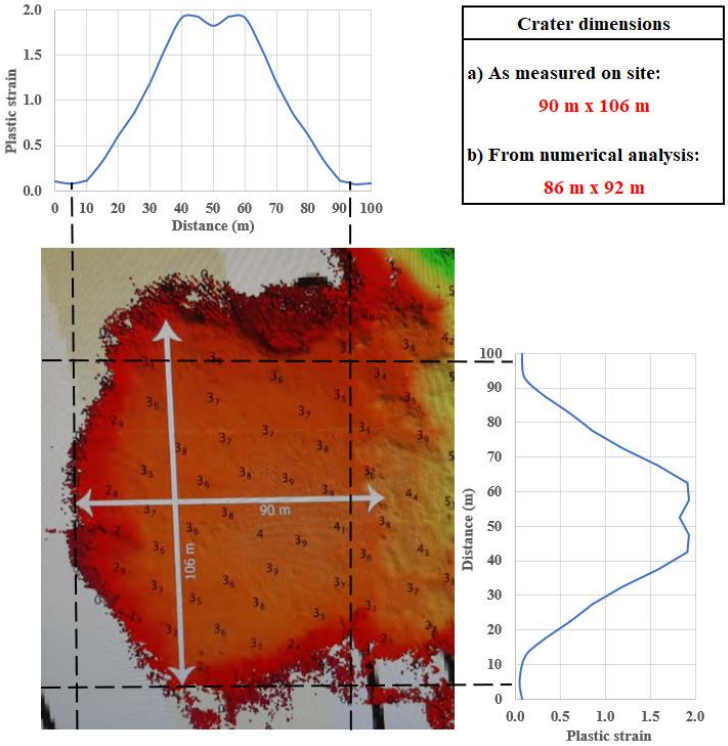

Figure 29: Crater dimensions as measured on site [46] vs numerical analysis

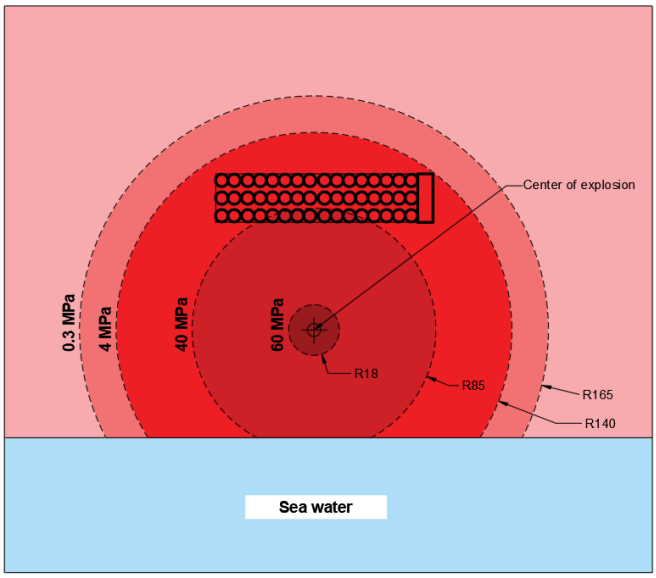

Figure 30: Ground stressed zone from the explosion (Radius in m)

Comparing results from CONWEP and CEL methods, it was realized that both methods led to similar explosive masses (210 t in CONWEP and 220 t in CEL). This is due to two main factors, the first is that blast waves in both methods propagate in hemispherical shape (surface explosion). The second is the absence of the clearing effect that typically reduces the positive phase duration of reflected pressures and therefore the impulse (Figure 31). The clearing effect is omitted in the CONWEP method for the finite dimension objects. For the case of Beirut explosion, the positive duration (t_{0H}=60 ms) is smaller than the positive clearing time (t_{0C}=185 ms), and therefore the reflected pressure was not affected by clearing.

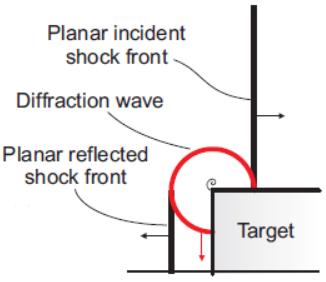

(a)

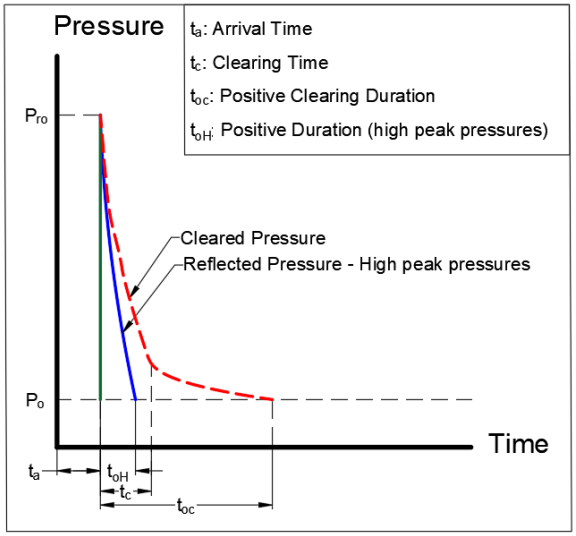

(b)

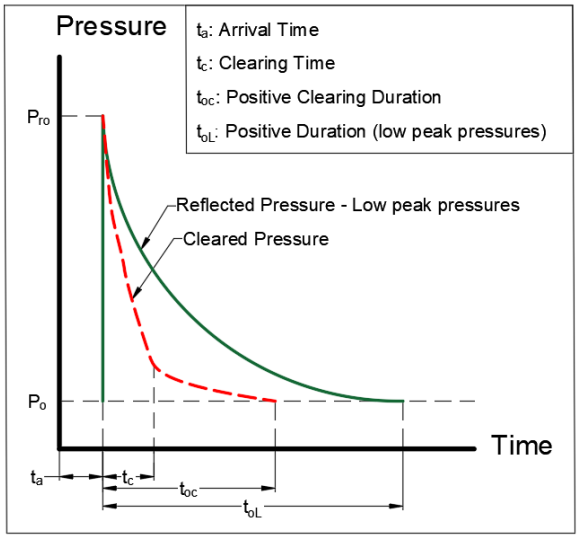

(c)

Figure 31: a) Clearing effect [47] b) The effect of clearance on the positive phase of high-peak reflected pressure curves

c) The effect of clearance on the positive phase of low-peak reflected pressure curves

4.3 Relevant Study Findings

4.3.1 Pressure Values and Peak Pressures

The blast pressure history from both CONWEP and CEL methods for silos is shown in Figure 32. The maximum peak pressure reaches a value of 2.63 MPa at 56 ms after detonation in CONWEP method, while it reaches a value of 2.89 MPa at 54 ms after detonation in CEL method. Using the UFC code [45], the peak blast pressure is 3.4 MPa. The difference is due to the complexity and irregularity of the silos' geometry (the code method is adequate to regular structure shapes).

After the sudden increase of the pressure, the wave decays exponentially until reaching minimum value at t =114 ms for both methods. The force and moment reactions resulting from the applied blast pressure at silo's base are 5.76×10^5 kN and 4.5×10^5 kN.m respectively from the CONWEP method, and 6.05×10^5 kN and 4.75×10^5 kN.m respectively from the CEL method. Moreover, the variation of peak blast pressure for each single silo of the remaining ones (14 silos) is shown in Figure 33 for both methods. Pressure values ranges from 1.14 MPa for silo number 1 to 2.63 MPa for silo number 11 in CONWEP method (refer to Figure 25 for silos numbering), while it ranges from 1.34 MPa for silo number 1 to 2.89 MPa for silo number 9 in CEL method. The construction second phase silos are subjected to higher blast pressures than first phase silos according to both methods due to the positioning of the blast detonation point, as mentioned earlier.

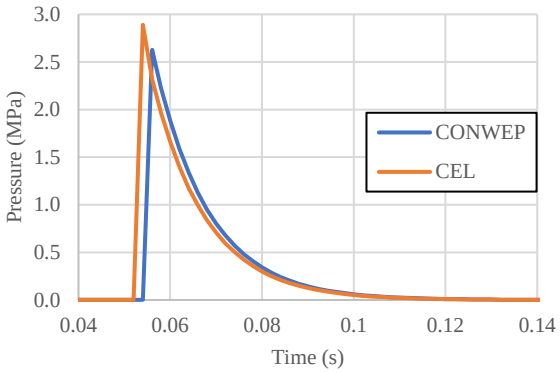

Figure 32: Blast pressure history (MPa)

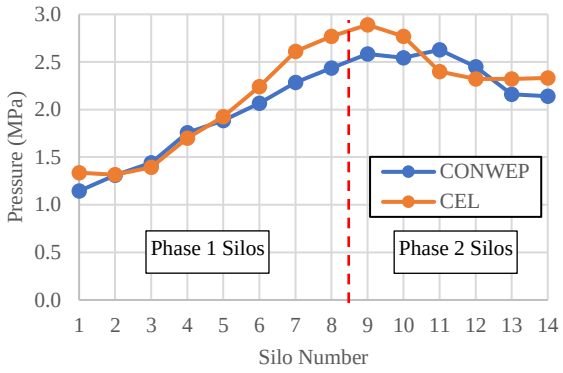

Figure 33: Peak blast pressure for remaining silos (MPa)

4.3.2 Z-Factor

One of the most important parameters in blast analysis is the scaled distance ratio" Z", which is a scale for blast events. When two blast events, with different standoff distance and equivalent mass of TNT, have the same Z, they produce the same peak pressure when hitting the object. The following Equation provides the scaled distance:

$$Z = \frac{d}{m_{TNT}^{1/3}} \quad (5)$$

Where *"d"* is the standoff distance (m) and *"m_{TNT}"* is the equivalent TNT mass of explosion (kg). Z factor enables the determination of explosion parameters -including the overpressure- from code charts. Based on the summarized results in Table 4, the scaled distance value for case 1 (1100 t of TNT) is 0.727m. This value is increased as the TNT mass decreased for the same standoff distance until reaching 2.036m for case 7 (50 t of TNT). For the determined value of exploded mass (equivalent TNT 220 t), the scaled distance is 1.242m.

Knowing the value of the scaled distance, and based on the code of practice, structural engineers can determine several blast parameters such as incident pressure, incident impulse, shock front velocity, and the required safety distances to protect people's lives. Furthermore, the pressure values on the surrounding buildings may be accurately estimated since the scaled distance obtained from finite element modeling is accurate for irregular structures. This will help in the rehabilitation process for the damaged buildings in the future.

4.3.3 The Strain Rate

The nature of the applied load (static or dynamic) may be defined with the strain rate value. According to Figure 34, strain rates above 1 s^{-1} are usually anticipated for impact and blast load cases. Strain rates between 1 s^{-1} to 100 s^{-1} are known as intermediate strain rates, whereas strain rates beyond 100 s^{-1} are known as high strain rates. Figure 35 plots the strain rate against the scaled distance for each case study, where the authors have derived the below exponential trend curve, to link both parameters for this case study as follows:

$$\dot{\epsilon} = 0.4 + 127.94e^{-4.908Z} \quad (6)$$

Where "$\dot{\epsilon}$" is strain rate (s^{-1}) and *"Z"* is the scaled distance ($m/kg^{1/3}$). The R^2 – factor for the Equation was around 0.985.

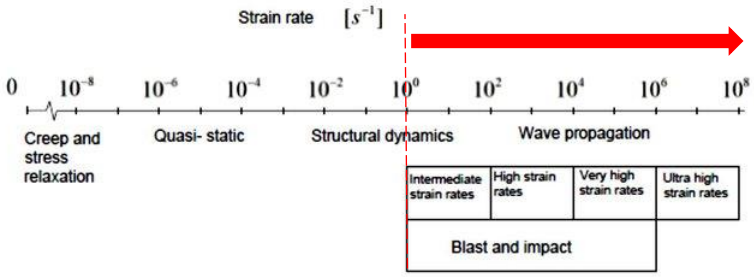

Figure 34: Strain rates for different loading conditions (s^{-1})

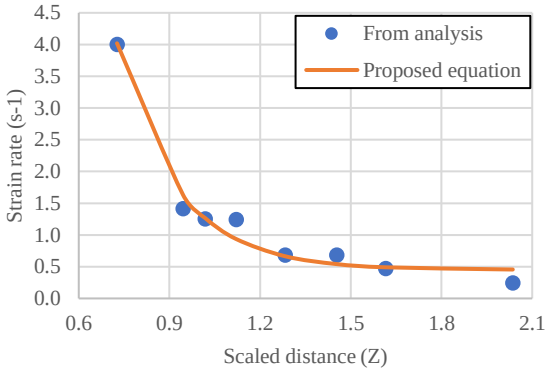

Figure 35: Scaled distance vs strain rate for each case study

4.3.4 The Projective Role of Silos

According to the UFC code [45], the total energy released by the explosion of 220 t of TNT equivalent is 9.2 x 10^{12} J. As for grain silos building, it dissipated only 2.58x10^{8} J according to CONWEP method and 9.8x10^{8} J according to CEL method. These values are relatively small compared to the total released energy by the explosion. Based on the above finding, the silos' protective role to the structures behind it is insignificant.

Figure 36 shows reinforced concrete and steel structures just behind the silos. Both structures were destroyed from the blast wave. This was also obtained from the numerical analysis of these two buildings behind the silos. It can also be noted that both structures were severely damaged and consequently failed. Moreover, this emphasizes the fact that the silos didn't play a significant role in protecting structures behind them (Figures 36c and 36d).

(a)

(b)

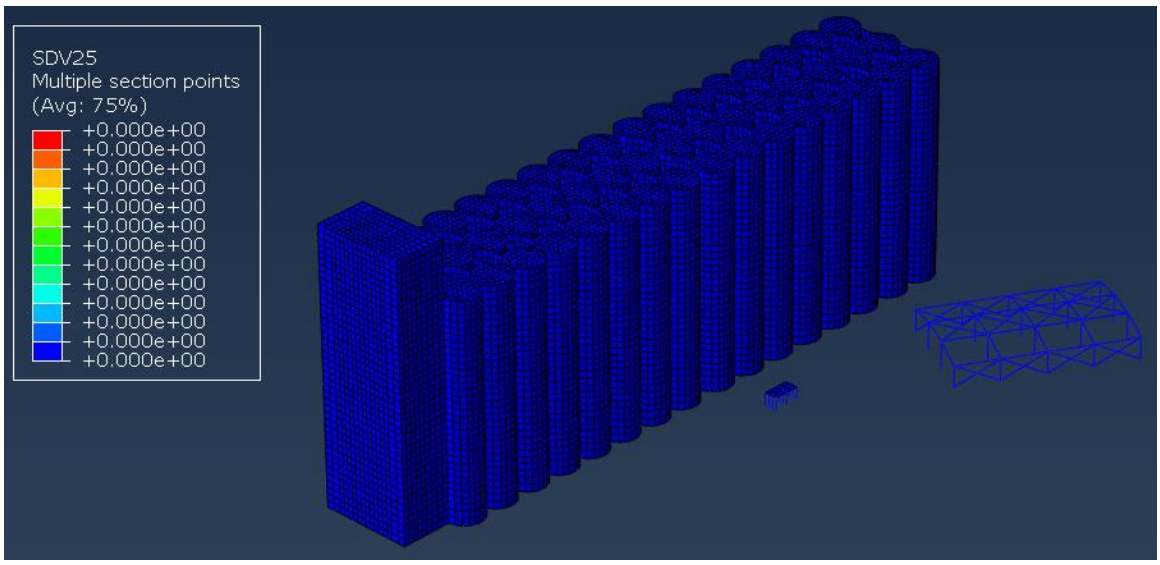

(c)

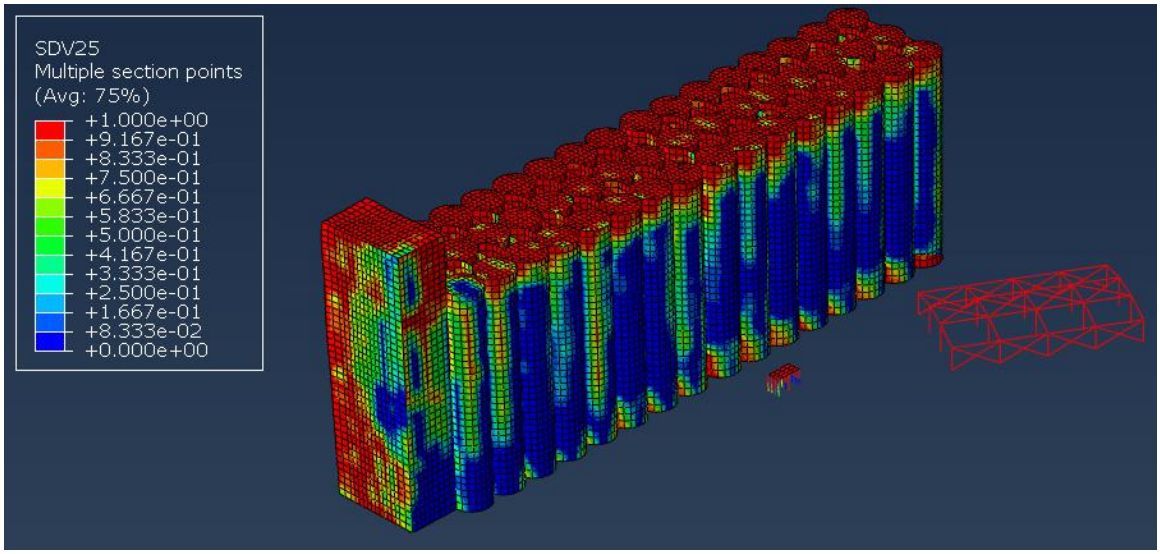

(d)

Figure 36: a) Structures behind the silos (before the explosion) b) Structures behind the silos (after the explosion)

c) Degree of damage for the silos and the structures behind before the explosion

d) Degree of damage for the silos and the structures behind after the explosion

4.3.5 The Structural State of the Remaining Silos

Based on this study, remaining silos experienced significant top and bottom damages (Figure 27) and large top sways (≈H/166), and are therefore considered unstable structures. In addition, the maximum applied tension and compression forces on silos by the explosion were compared to the axial tension and compression capacity in both vertical and horizontal directions as shown in Figure 37. In tension, the maximum applied tensile forces in all silos exceeded the capacity in both vertical direction (574 kN) and horizontal direction (1104 kN). Similar trend is realized for forces in compression, where the applied forces in both directions were higher than capacities in both vertical direction (6465 kN) and horizontal direction (6971 kN). Referring to the previous analysis, it is recommended to demolish the remaining silos or to apply major strengthening works to keep them.

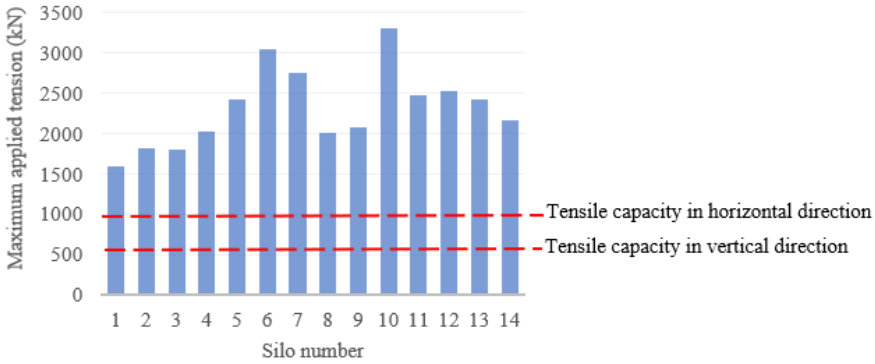

(a)

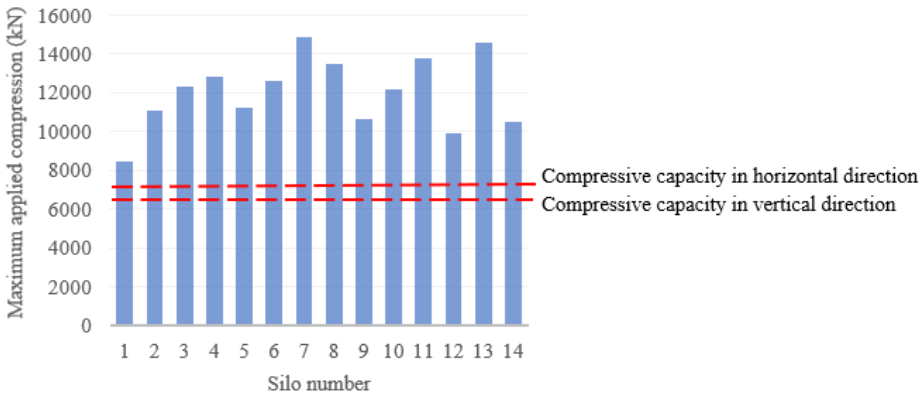

(b)

Figure 37: a) Tensile capacity vs applied force for remaining silos

b) Compressive capacity vs applied force for remaining silos

4.3.6 Mesh Sensitivity Analysis

Several mesh sizes for the Eulerian domain were tested to ensure the accuracy of the results; hence stressing the credibility of the numerical model. Several numerical analyses were performed for mesh sizes of 9 m, 7.5 m, 6 m, 4.5 m, 3 m, 1.5 m, 1 m, and 0.75 m respectively. The results show that as the mesh gets coarser, the equivalent required TNT mass to cause the same degree of damage and lateral sway decreases. For example, a mesh size of 9 m leads to an equivalent TNT mass of 170 t. As the mesh gets finer, the change rate of the TNT mass increases reaching 220 t for mesh size $\leq$ 3 m (Figure 38). Therefore, the authors have adopted the 3 m mesh size to minimize the analysis time without affecting the accuracy of results.

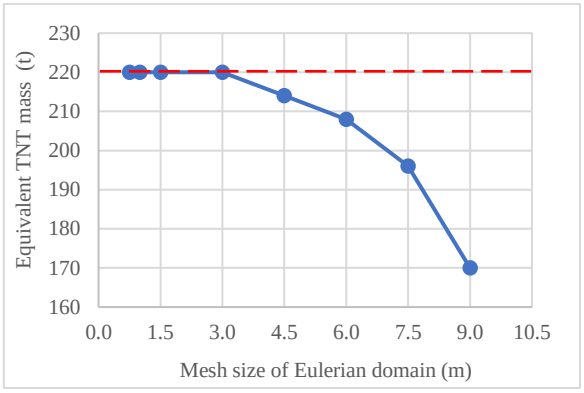

Figure 38: The equivalent TNT mass for Beirut explosion vs the mesh size of the Eulerian domain.

5. Conclusions

Non-linear numerical modeling for grain silos was conducted to study the structural response to massive blast loading with Beirut explosion as a case study. Exact geometry and material inputs were determined from detailed drawings and site investigations. The numerical analysis was performed throughout several finite element models, with variation of blast generation methods (CONWEP and CEL). A details analysis was conducted to evaluate different findings related to the blast magnitude and silos' structural response. The results of this study led to the following conclusions:

1- The analysis results prove that an amount equivalent to 220 t of TNT (or 564 t of AN) is adequate to generate damages similar to those resulting from the explosion. This amount represents 20.5% of the original stored amount (2750 t). This is close to the quantities resulting from recent studies conducted by Dewey [29], Herbert [30], and Lewis [31] on Beirut explosion, which resulted in the average percentage of exploded equivalent TNT quantity as 27%, 23%, and 32% respectively.

2- As a result of the explosion, the silos had been subjected to a peak blast pressure of 2.89 MPa (resulting from 220 t of TNT equivalent). The time elapsed for the blast wave to reach the structure was 54ms, generating a blast pressure distribution that ranges from 1.34 MPa for Silo number 1 to 2.89 MPa for Silo number 9.

3- The scaled distance factor (Z) for Beirut blast case is 1.242 m. This value is very important for structural studies related to the silos, since it enables designers to determine different blast parameters such as: wave shock speed, incident pressure, reflected pressure, and dynamic pressure.

4- In Beirut blast case, the total work dissipated by the silos is 9.8×10^8J. This value is important to determine the amount of energy absorbed by the silos, which is around 0.11% of the total released energy by 220 t of TNT equivalent mass. This refutes the claims that the silos protected Beirut city from total destruction.

5- In this case study, the explosion was strong enough that no clearing effect took place. This justifies the reason behind the close estimations between the CONWEP method and the CEL method, where the difference between the estimated explosive mass is 4.5% only.

6- Regarding the current condition of silos, they are considered as structurally unstable. This was shown by comparing the maximum applied tensile and compressive forces in both vertical and horizontal directions to the capacity in each direction. The applied tensile forces were 6 times higher than the tensile capacity, while the applied compressive forces were 2 times higher than the compressive capacity.

6. Recommendations

1. Due to the enormous hazards resulting from explosions on common residential building structures, and considering the relatively high-cost impact in designing buildings to resist blast, it is strongly recommended to relocate storage zones of explosive materials and buildings prone to explosions away from residential zones.
2. For complex geometries, it is highly recommended to perform finite element analysis since code estimations are basically adequate for regular shape structures. This was realized in the current study when the peak pressure value calculated by numerical analysis exceeded that calculated from UFC code equations by around 23%.
3. Due to the uncertainty related to blast main factors (explosion nature, weight of explosive material, and stand-off distance) and the relatively high blast pressure, it is recommended to consider blast protection structures, such as RC walls or a shock absorber system (Aluminum foams or others) installed on the structures front face, for vital structures that are prone to accidental explosion incidents. The walls or the shock absorber system may absorb most of the energy released by an explosion; therefore, protected structures can be repaired and reused without the need for reconstruction as in the case in Beirut silos.

References

1. Temsah, Y., Jahami, A., Khatib, J., & Sonebi, M. (2018). Numerical analysis of a reinforced concrete beam under blast loading. MATEC Web of Conferences, 149, 02063. https://doi.org/10.1051/matecconf/201814902063
2. Temsah, Y., Jahami, A., Khatib, J., & Sonebi, M. (2018). Numerical Derivation of Iso-Damaged Curve for a Reinforced Concrete Beam Subjected to Blast Loading. MATEC Web of Conferences, 149, 02016. https://doi.org/10.1051/matecconf/201814902016
3. Jahami, A., Temsah, Y., & Khatib, J. (2019). The efficiency of using CFRP as a strengthening technique for reinforced concrete beams subjected to blast loading. International Journal of Advanced Structural Engineering, 11(4), pp.411–420. https://doi.org/10.1007/s40091-019-00242-w.
4. Jahami, A., Temsah, Y., Khatib, J., Baalbaki, O., Kenai, Said. (2021). The behavior of CFRP strengthened RC beams subjected to blast loading. Magazine of Civil Engineering, 103(3). DOI: 10.34910/MCE.103.9.
5. Zhang, D., Yao, S. J., Lu, F., Chen, X. G., Lin, G., Wang, W., & Lin, Y. (2013). Experimental study on scaling of RC beams under close-in blast loading. Engineering Failure Analysis, 33, pp.497–504. https://doi.org/10.1016/j.engfailanal.2013.06.020
6. Al Rawi, Y., Temsah, Y., Baalbaki, O., Jahami, A., & Darwich, M. (2020). Experimental investigation on the effect of impact loading on behavior of post- tensioned concrete slabs. Journal Of Building Engineering, 101207. doi: 10.1016/j.jobe.2020.101207.
7. Jahami, A., Temsah, Y., Khatib, J., Baalbaki, O., Darwiche, M., Chaaban, S. (2020) Impact behavior of rehabilitated post-tensioned slabs previously damaged by impact loading. Magazine of Civil Engineering. 93(1). Pp. 134–146. DOI: 10.18720/MCE.93.11.
8. Jahami, A., Temsah, Y., Khatib, J., Baalbaki, O., Sonebi, M. (2020). Strengthening of post-tensioned slab subjected to impact loading. In: 74th RILEM Annual Week & 40th Cement and Concrete Science Conference. University of Sheffield, Sheffield, UK.
9. Jahami, A., Temsah, Y., Baalbaki, O., Darwiche, M., Al-Rawi, Y., Al-Ilani, M. & Chaaban, S. (2019) Effect of Successive Impact Loads From a Drop Weight on a Reinforced Concrete Flat Slab. MATEC Web of Conferences, 281, 02003. DOI: https://doi.org/10.1051/matecconf/201928102003.
10. Jahami, A., Temsah, Y., Khatib J., Sonebi M. (2018) Numerical Study For The Effect of Carbon Fiber Reinforced Polymers (CFRP) Sheets on Structural Behavior of Posttensioned Slab Subjected to Impact Loading, Proceedings of the Symposium on Concrete Modelling – CONMOD2018 , RILEM PRO 127, Edited by Erik Schlangen et al., pp. 259-267.
11. Temsah, Y., Jahami, A., Khatib, J. and Firat, S. (2017). Numerical study for RC beams subjected to blast waves. In: 1st International Turkish World Engineering and Science Congress in Antalya. Antalya, Turkey.
12. Temsah, Y., Jahami, A., Khatib, J. and Firat, S. (2017). Single Degree of Freedom Approach of a Reinforced Concrete Beam Subjected to Blast Loading. In: 1st International Turkish World Engineering and Science Congress in Antalya. Antalya, Turkey.
13. Anas, S., Alam, M. and Umair, M. (2021). Experimental and numerical investigations on performance of reinforced concrete slabs under explosive-induced air-blast loading: A state-of-the-art review. Structures, 31, pp.428-461.
14. Wu, C., Oehlers, D., Rebentrost, M., Leach, J. and Whittaker, A., 2009. Blast testing of ultra-high performance fibre and FRP-retrofitted concrete slabs. Engineering Structures, 31(9), pp.2060-2069.

15. Castedo, R., Segarra, P., Alañon, A., Lopez, L., Santos, A. and Sanchidrian, J., 2015. Air blast resistance of full-scale slabs with different compositions: Numerical modeling and field validation. International Journal of Impact Engineering, 86, pp.145-156.
16. Zhao, C., Lu, X., Wang, Q., Gautam, A., Wang, J. and Mo, Y., 2019. Experimental and numerical investigation of steel-concrete (SC) slabs under contact blast loading. Engineering Structures, 196, p.109337.
17. Schenker, A., Anteby, I., Gal, E., Kivity, Y., Nizri, E., Sadot, O., Michaelis, R., Levintant, O. and Ben-Dor, G., 2008. Full-scale field tests of concrete slabs subjected to blast loads. International Journal of Impact Engineering, 35(3), pp.184-198.
18. Yan, J., Liu, Y., Xu, Z., Li, Z. and Huang, F., 2020. Experimental and numerical analysis of CFRP strengthened RC columns subjected to close-in blast loading. International Journal of Impact Engineering, 146, p.103720.
19. Lee, J., Aoude, H., Yoon, Y. and Mitchell, D., 2020. Impact and blast behavior of seismically-detailed RC and UHPFRC-Strengthened columns. International Journal of Impact Engineering, 143, p.103628.
20. Li, Z., Zhang, X., Shi, Y., Wu, C. and Li, J., 2021. Finite element modeling of FRP retrofitted RC column against blast loading. Composite Structures, 263, p.113727.
21. Zhang, F., Wu, C., Li, Z. and Zhao, X., 2021. Residual axial capacity of CFDST columns infilled with UHPFRC after close-range blast loading. Thin-Walled Structures, 96, pp. 314-327.
22. Chen, Z., Li, X., Yang, Y., Zhao, S., & Fu, Z. (2018). Experimental and numerical investigation of the effect of temperature patterns on behaviour of large scale silo. Engineering Failure Analysis, 91(October 2017), pp.543–553. https://doi.org/10.1016/j.engfailanal.2018.04.043
23. Elghazouli, A. Y., & Rotter, J. M. (1996). Long-term performance and assessment of circular reinforced concrete silos. Construction and Building Materials, 10(2), 117–122. https://doi.org/10.1016/0950-0618(95)00091-7
24. Gallego, E., González-Montellano, C., Ramírez, A., & Ayuga, F. (2011). A simplified analytical procedure for assessing the worst patch load location on circular steel silos with corrugated walls. Engineering Structures, 33(6), pp.1940–1954. https://doi.org/10.1016/j.engstruct.2011.02.032
25. Giuliani, F., De Falco, A., Landi, S., Giorgio Bevilacqua, M., Santini, L., & Pecori, S. (2018). Reusing grain silos from the 1930s in Italy. A multi-criteria decision analysis for the case of Arezzo. Journal of Cultural Heritage, 29, pp.145–159. https://doi.org/10.1016/j.culher.2017.07.009
26. Hulimka, J., & Kałuża, M. (2019). A history of failure and repairs of the reinforced concrete raw coal silo. Engineering Failure Analysis, 104(April), 657–672. https://doi.org/10.1016/j.engfailanal.2019.06.019
27. Matiaskova, L., Bilcik, J., & Soltesz, J. (2020). Failure analysis of reinforced concrete walls of cylindrical silos under elevated temperatures. Engineering Failure Analysis, 109(May), 104281. https://doi.org/10.1016/j.engfailanal.2019.104281
28. Rigby, S., Lodge, T., Alotaibi, S., Barr, A., Clarke, S., Langdon, G. and Tyas, A. (2020). Preliminary yield estimation of the 2020 Beirut explosion using video footage from social media. Shock Waves, 30(6), pp.671-675.
29. Dewey, J. (2021). The TNT and ANFO equivalences of the Beirut explosion. Shock Waves.
30. Reuters. 2021. How powerful was the Beirut blast?. [online] Available at: <https://graphics.reuters.com/LEBANON-SECURITY/BLAST/yzdpxnmqbpx/> [Accessed 2 April 2021].
31. Business Insider. 2021. The deadly explosion that devastated Beirut appears to have been far more powerful than the 'Mother of All Bombs'. [online] Available at: <https://www.businessinsider.com/how-big-was-the-explosion-that-devastated-beirut-moab-2020-8> [Accessed 2 April 2021].
32. Sika Near East for construction chemicals. Rehabilitation of Silos - Beirut Port. (2002). Beirut, Lebanon.
33. ASTM C42 / C42M-20, Standard Test Method for Obtaining and Testing Drilled Cores and Sawed Beams of Concrete, ASTM International, West Conshohocken, PA, 2020, www.astm.org. DOI: 10.1520/C0042_C0042M-20.
34. ASTM C496 / C496M-17, Standard Test Method for Splitting Tensile Strength of Cylindrical Concrete Specimens, ASTM International, West Conshohocken, PA, 2017, www.astm.org. DOI: 10.1520/C0496_C0496M-17.
35. ACI 318-14, Building code requirements for structural concrete. Farmington Hills, Michigan: American Concrete Institute, ACI. 2014.
36. ASTM A615 / A615M-20, Standard Specification for Deformed and Plain Carbon-Steel Bars for Concrete Reinforcement, ASTM International, West Conshohocken, PA, 2020, www.astm.org. DOI: 10.1520/A0615_A0615M-20.
37. AMANN. (2020). Technical Support Beyrouth. Beirut.
38. MC90 (1993) CEB-FIP Model Code 1990, Design code, 6th edn, Thomas Telford, Lausanne, Switzerland.
39. Kamali, A. (2012). Shear Strength of Reinforced Concrete Beams subjected to Blast Loading. Master of Science. Royal Institute of Technology (KTH).
40. Density of Wheat in 285 units of density. (2020). Retrieved 11 October 2020, from https://www.aqua-calc.com/page/density-Table/substance/wheat#:~:text=Density%20of%20Wheat%20(material)&text=Wheat%20weighs%200.769%20gram%20per,inch%20%5Boz%2Finch%C2%B3%5D%20.
41. Khodabakhshian, R., & Emadi, B. (2011). Determination of the modulus of elasticity in agricultural seeds on the basis of elasticity theory. Middle-East Journal of Scientific Research, 7(3), 367–373. http://www.idosi.org/mejsr/mejsr7(3)11/19.pdf.
42. Lawton, P. J. (1980). Coefficients of friction between cereal grain and various silo wall materials. Journal of Agricultural Engineering Research, 25(1), 75–86. https://doi.org/10.1016/0021-8634(80)90049-9.
43. Botez, M.D., Bredean, L.A. Numerical Study of a RC Slab Subjected to Blast: A Coupled Eulerian-Lagrangian Approach (2019). IOP Conference Series: Materials Science and Engineering. 471(5). DOI:10.1088/1757-899X/471/5/052036.
44. Hibbitt, Karlsson, Sorensen, 2011, ABAQUS User's Manual, Pawtucket, 6th Edition.
45. UFC 3-340-02, (2008). Structures to resist the effects of accidental explosions, Department of Defense, USA, 2008
46. Khatib & Alami. (2020). Beirut harbor silos technical report. [online] pp.59-60. Available at: <http://www.khatibalami.com> [Accessed 2 February 2021].
47. Rigby, S. (2014). *Blast Wave Clearing Effects on Finite-Sized Targets Subjected to Explosive Loads* (Ph.D.). University of Sheffield.